Gas Phase S_N2 Reactions of Halide Ions with Trifluoromethyl Halides: Front- and Back-Side Attack *vs.* Complex Formation†

B. Bogdanov and T. B. McMahon*

Department of Chemistry, University of Waterloo, Waterloo, Ontario N2L 3G1, Canada

Received: July 25, 2005; In Final Form: November 16, 2005

Density functional theory computations and pulsed-ionization high-pressure mass spectrometry experiments have been used to explore the potential energy surfaces for gas-phase S_N2 reactions between halide ions and trifluoromethyl halides, $X^- + CF_3Y \rightarrow Y^- + CF_3X$. Structures of neutrals, ion−molecule complexes, and transition states show the possibility of two mechanisms: back- and front-side attack. From pulsed-ionization high-pressure mass spectrometry, enthalpy and entropy changes for the equilibrium clustering reactions for the formation of $Cl^-(BrCF_3)$ (-16.5 ± 0.2 kcal mol^{-1} and -24.5 ± 1 cal mol^{-1} K^{-1}), $Cl^-(ICF_3)$ (-23.6 ± 0.2 kcal mol^{-1}), and $Br^-(BrCF_3)$ (-13.9 ± 0.2 kcal mol^{-1} and -22.2 ± 1 cal mol^{-1} K^{-1}) have been determined. These are in good to excellent agreement with computations at the B3LYP/6-311+G(3df)//B3LYP/6-311+G(d) level of theory. It is shown that complex formation takes place by a front-side attack complex, while the lowest energy S_N2 reaction proceeds through a back-side attack transition state. This latter mechanism involves a potential energy profile which closely resembles a condensed phase S_N2 reaction energy profile. It is also shown that the $Cl^- + CF_3Br \rightarrow Br^- + CF_3Cl$ S_N2 reaction can be interpreted using Marcus theory, in which case the reaction is described as being initiated by electron transfer. A potential energy surface at the B3LYP/6-311+G(d) level of theory confirms that the $F^- + CF_3Br \rightarrow Br^- + CF_4$ S_N2 reaction proceeds through a Walden inversion transition state.

Introduction

Bimolecular nucleophilic displacement (S_N2) reactions in the gas phase between halide ions and halomethanes, eq 1, have been studied extensively for over three decades, both experimentally[1−25] and theoretically, using electronic structure[26−47] and trajectory[48−69] computations.

$$X^- + CH_3Y \rightarrow XCH_3 + Y^- \quad (1)$$

In the condensed phase, this type of reaction had already received substantial attention from the 1930s onward, initially by Ingold and co-workers,[70] and followed by many others.[71−73] The S_N2 acronym comes from the fact that the rate of reaction is first-order both in the nucleophile and substrate concentrations, $[X^-]$ and $[CH_3Y]$, respectively, eq 2, making the overall reaction second order.

$$\text{rate} = k[X^-][CH_3Y] \quad (2)$$

In Figure 1, a typical schematic potential energy profile is shown for an exothermic, condensed phase S_N2 reaction. Because of the high central barrier of 15−30 kcal mol^{-1}, most reactions proceed very slowly. This is mainly caused by strong solvation effects, which mask the intrinsic reactivity of the species involved. By performing S_N2 reactions in the gas phase, information on intrinsic energetics, dynamics, and kinetics can be obtained, thereby exposing the role of the solvent in condensed phase reactions. Many experiments and computations have shown that in the gas-phase S_N2 reactions proceed through a double-well potential,[6] such as that shown in Figure 2. A large variety of rates and reaction efficiencies have been observed and these are mainly due to variations in the central barrier height relative to the reactants.

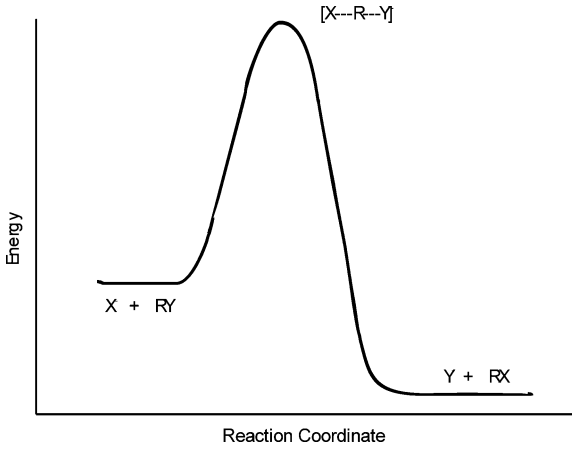

Figure 1. Hypothetical potential energy surface for a condensed phase S_N2 reaction.

The gas-phase S_N2 reaction is thus proposed to proceed by three consecutive, elementary processes: (i) formation of an entrance channel ion−molecule complex from the reactants, eq 3; (ii) conversion of the entrance channel ion−molecule complex to the exit channel ion−molecule complex through a transition state, eq 4; (iii) dissociation of the exit channel ion−molecule complex into the products, eq 5.

† Part of the special issue "William Hase Festschrift".

* Corresponding author. Telephone: (519) 888-4591. Fax: (519) 746-0435. E-mail: mcmahon@Uwaterloo.ca.

10.1021/jp0541011 CCC: $33.50
Published on Web 01/11/2006

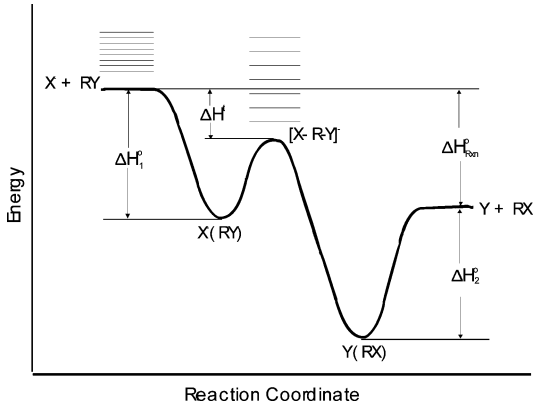

Figure 2. Hypothetical double minimum potential energy surface for a gas-phase S_N2 reaction.

$$X^- + CH_3Y \rightleftharpoons X^-(CH_3Y) \quad (3)$$

$$X^-(CH_3Y) \rightleftharpoons [X\cdots CH_3\cdots Y]^{-\ddagger} \rightleftharpoons Y^-(CH_3X) \quad (4)$$

$$Y^-(CH_3X) \rightleftharpoons Y^- + CH_3X \quad (5)$$

The transition state is represented by $[XCH_3Y]^{-\ddagger}$, indicating synchronous shortening and lengthening of the X−C and C−Y bonds, respectively. Under thermal, low-pressure conditions, S_N2 reactions are initiated via the so-called back-side attack mechanism as indicated by eq 3.

From many experiments and trajectory computations, it has been shown that the energy redistribution in the entrance channel ion−molecule complex may be nonstatistical.[13,15,16,49,52−54,56,60,63,74−78] This is ascribed as being due to the short lifetime of the nascent complex and the poor energy transfer between the intermolecular and intramolecular vibrational modes of the complex. As a consequence of this, it had been conjectured that the neutral CH_3X product could then be vibrationally excited.[13]

Barlow et al. studied the rate coefficient for eq 6 as a function of the kinetic energy of $^{37}Cl^-$ using a flowing afterglow-selected ion flow tube (FA-SIFT) apparatus, and observed an exponential increase in the rate constant with increasing ion energy from 0.4 to 2.0 eV.[79]

$$^{37}Cl^- + CH_3{}^{35}Cl \rightarrow {}^{35}Cl^- + CH_3{}^{37}Cl \quad (6)$$

This result was explained by assuming the occurrence of a higher energy mechanism with a $[CH_3{}^{35}Cl{}^{37}Cl]^{-\ddagger}$ transition state, in which the two chlorine atoms are equivalent. The possibility of such a front-side attack mechanism has been examined experimentally by Johnson and co-workers,[11,80−83] and Ervin and co-workers,[15] and theoretically by the groups of Radom,[39] Hase,[38] and Ziegler.[36]

Cyr et al.[80] observed, besides formation of displacement reaction products, formation of $ClBr^{-\bullet}$ and $I_2^{-\bullet}$ for eqs 7 and 8 at elevated center-of-mass kinetic energies of the nucleophiles.[80] Johnson and co-workers further observed a higher energy identity reaction

$$Cl^- + CH_3Br \rightarrow ClBr^{-\bullet} + CH_3^\bullet \quad (7)$$

$$I^- + CH_3I \rightarrow I_2^{-\bullet} + CH_3^\bullet \quad (8)$$

channel for $I_a^-(CH_3I_b)$ and formation of $BrI^{-\bullet}$ from $I^-(CH_2Br_2)$ upon photoexcitation, eqs 9 and 10.[11,81−83]

$$I_a^-(CH_3I_b) + h\nu \rightarrow I_a^- + CH_3^\bullet + I_b^\bullet \quad (9)$$

$$I^-(CH_2Br_2) + h\nu \rightarrow BrI^{-\bullet} + CH_2Br^\bullet \quad (10)$$

Ervin and co-workers have also investigated eq 6[15] and eq 7[77] using guided ion beam tandem mass spectrometry techniques, (GIB-MS/MS) and observed a process that closely resembled the results of Barlow et al.[79] in the case of the former reaction. However rigorous statistical modeling indicated that the observed reaction proceeded via back-side attack. In addition, formation of $Cl_2^{-\bullet}$ was observed at a center of mass kinetic energy, E_{cm}, of 4.3 ± 0.4 eV (99 ± 9 kcal mol^{-1}), eq 11.

$$^{37}Cl^- + CH_3{}^{35}Cl \rightarrow {}^{35}Cl{}^{37}Cl^{-\bullet} + CH_3^\bullet \quad (11)$$

In a subsequent study of the reaction between fluoride ion and methyl chloride, both proton abstraction and formation of $FCl^{-\bullet}$ were observed at higher center-of-mass kinetic energies of F^-, in addition to the S_N2 reaction, eqs 12−14.[25a] In their examination of eq 7,[77] they were able to show that this reaction behaves

$$F^- + CH_3Cl \rightarrow Cl^- + CH_3F \quad (12)$$

$$F^- + CH_3Cl \rightarrow CH_2Cl^- + HF \quad (13)$$

$$F^- + CH_3Cl \rightarrow FCl^{-\bullet} + CH_3^\bullet \quad (14)$$

statistically at thermal energies, in contrast to earlier suggestions that this reaction might behave nonstatistically.[13] Radom and co-workers have shown that at the G2(+) level of theory the back-side attack transition state, $[ClCH_3Cl]^{-\ddagger}$, is 2.7 kcal mol^{-1} higher in energy than the reactants,[37] in good agreement with experimental results, while the front-side attack transition state, $[CH_3Cl_2]^{-\ddagger}$, is 46.3 kcal mol^{-1} higher in energy.[39] Interestingly, the $[CH_3Cl_2]^{-\ddagger}$ front-side attack transition state was formed from the back-side attack complex, $Cl^-(CH_3Cl)$, rather than from the front-side attack complex, $Cl^-(ClCH_3)$, since this latter complex was not located as a stable minimum. In contrast, stable minima were located for the $Br^-(BrCH_3)$ and $I^-(ICH_3)$ front-side attack complexes at the G2(+)(ECP) level of theory.[39] The binding energies for these two complexes are however much lower than those for the back-side attack complexes, $Br^-(CH_3Br)$ and $I^-(CH_3I)$, with values of 1.7 kcal mol^{-1} vs 9.8 kcal mol^{-1} and 4.6 kcal mol^{-1} vs 8.6 kcal mol^{-1}, respectively.

Halide ion−halogen interactions are not unknown in chemistry, with, for example, the gas-phase trihalide anions, X_3^- (X = F, Cl, Br, I), existing as hypervalent species with true covalent bonds. [84] Recently the bond dissociation energies were determined for these four species with values of 23.5 ± 2.5 kcal mol^{-1} for F_3^-,[84] 23.6 ± 1.2 kcal mol^{-1} for Cl_3^-, [85] 30.3 ± 1.7 kcal mol^{-1} for Br_3^-,[85] and 30.1 ± 1.4 kcal mol^{-1} for I_3^- [86] having been obtained. Recent photodissociation experiments and DFT computations on $BrICl^-$ and $BrIBr^-$ also reveal interesting dynamics and chemistry for these novel species.[87]

In view of the above findings, it would seem reasonable to assume that by replacing the CH_3 with a CF_3 group it may be possible to render front-side attack more energetically accessible, in which case it might become the main mechanism for the S_N2 reaction. The electronic repulsion between the nucleophile and the electronegative fluorine atoms would also logically impede back-side attack from taking place. There are only a relatively small number of articles published concerning ion−molecule reactions between halide ions (and other anions) and trifluoromethyl halides. Hop and McMahon studied the endothermic S_N2 reaction between bromide ion and dichlorodifluo-

romethane using Fourier transform ion cyclotron resonance (FT-ICR) threshold collision induced dissociation measurements, eq 15.[88]

$$Br^- + CF_2Cl_2 \rightarrow Cl^- + CF_2ClBr \qquad (15)$$

By following the abundance of the chloride ion as a function of the center-of-mass kinetic energy of the bromide ion, the threshold energy was obtained after analyzing the data using the empirical threshold model developed originally by Armentrout and co-workers [89] and a threshold value of 21.0 ± 1.2 kcal mol^{-1} was obtained. In that work, it had been speculated that the reaction proceeded through a front-side attack mechanism, involving a pentacoordinate transition state $[CF_2Cl_2Br]^{-\ddagger}$. Further it was conjectured that "the rapid and linear increase in cross-section at energies slightly above the threshold suggests nonstatistical behavior" and "a collision complex which is either not bound or very weakly bound" was implicated.

Morris and Viggiano studied the reactions of oxide ($O^{-\bullet}$) and superoxide ($O_2^{-\bullet}$) anions, and halide ions (X^-) with various trifluoro methyl halides (CF_3X) using a variable temperature (VT) SIFT instrument.[90] A wide variety of products was observed and the associated rate constants and reaction efficiencies were obtained. For these reactions between halide ions and trifluoro methyl halides, formation of adduct ions was observed, eqs 16 and 17, as well as formation of Br^- and I^-, eq 18. In general, the efficiencies for these reactions were quite low,

$$F^- + CF_3X \rightarrow F^-(XCF_3) \quad (X = Cl, Br, I) \qquad (16)$$

$$X^- + CF_3X \rightarrow X^-(XCF_3) \quad (X = Cl, Br, I) \qquad (17)$$

$$F^- + CF_3X \rightarrow X^- + CF_4 \quad (X = Br, I) \qquad (18)$$

with the exception of eq 18, for X = Br and I. In a subsequent study, Morris and Viggiano investigated the latter two reactions further as a function of temperature, kinetic energy, internal temperature, and pressure using the VT-SIFT instrument.[91] Under all conditions, the association reaction was the major reaction channel. From the results obtained, it was concluded that these reactions proceed by two different, noncompeting complexes and that the displacement reaction proceeds statistically by the classical Walden inversion mechanism.

In a further study using the SIFT apparatus, Morris et al. investigated the reactions between a large variety of anions, A^-, and the four trifluoro methyl halides (CF_3X) at 300 K.[92] Nonreactivity and complex formation were observed, as well as reactions initiated by electron transfer, which in most cases were fast and efficient.

Staneke et al. performed FT-ICR experiments between various negative ions and fluorochloro- and fluorobromomethanes.[93] For the reactions between OH^- and CF_3Cl and CF_3Br no formation of Cl^- or Br^- was observed. Formation of the adduct ion, $Br^-(BrCF_3)$, was observed, albeit from secondary reactions, eqs 19 and 20.

$$CF_3Br^{-\bullet} + CF_3Br \rightarrow CF_3^{-\bullet} + CF_3Br_2^- \qquad (19)$$

$$CH_3SHBr^- + CF_3Br \rightarrow CH_3SH + CF_3Br_2^- \qquad (20)$$

Surprisingly, no thermochemical data for the formation of the $F^-(XCF_3)$ and $X^-(XCF_3)$ complexes (X = Cl, Br, I) have been determined to date, either experimentally or computationally. In addition, no data are available on the thermochemistry of the transition states for either back- or front-side attack. Even though replacing the CH_3 group by a CF_3 group appears to favor formation of a front-side attack complex, it cannot be ruled out a priori that back-side attack is not possible, or even still more favorable for an S_N2 reaction, as was suggested by Morris and Viggiano.[91]

In the present work the thermochemistry for the equilibrium clustering reactions of chloride and bromide ions onto trifluoromethyl bromide and iodide, eqs 21−23, have been studied by pulsed ionization high-pressure mass spectrometry (PHPMS). In addition, high level DFT and ab initio computations have

$$Cl^- + CF_3Br \rightleftharpoons Cl^-(BrCF_3) \qquad (21)$$

$$Br^- + CF_3Br \rightleftharpoons Br^-(BrCF_3) \qquad (22)$$

$$Cl^- + CF_3I \rightleftharpoons Cl^-(ICF_3) \qquad (23)$$

been performed to gain further insight into the structures of the ion−molecule complexes and the transition states, and to construct potential energy profiles for the front- and back-side attack mechanisms, as well as other possible mechanisms. The quality of the calculated thermochemistry has also been evaluated by the agreement with the limited experimental data available to date.

Experimental Methods

All measurements were carried out on a pulsed-ionization high-pressure mass spectrometer (PHPMS), configured around a VG 8-80 mass spectrometer. The instrument, constructed at the University of Waterloo, has been described in detail previously.[94]

Gas mixtures were prepared manometrically in a 5 L heated stainless steel reservoir at 370 K, using CH_4 as the major gas at pressures of 700−800 Torr. In cases where small partial pressures of the CF_3X reactant were required, manometric dilutions of mixtures of known partial pressures were made by reducing the total pressure by a factor of 10−50 and then adding methane to a new, higher pressure. Chloride ion was generated from trace amounts of CCl_4 by dissociative electron capture of thermalized electrons from 50 to 500 μs pulses of a 2 keV electron gun beam. Bromide ion was efficiently generated by an S_N2 reaction between Cl^- and *n*-butyl bromide, eq 24.

$$Cl^- + CH_3CH_2CH_2CH_2Br \rightarrow Br^- + CH_3CH_2CH_2CH_2Cl \qquad (24)$$

The trifluoromethyl halides (CF_3Cl, CF_3Br or CF_3I) were added to the 5 L reservoir to give relative amounts between 0.1% and 1.6%, depending on the ion source temperature and the nature of the experiment involved. The ion source pressure and temperature ranged from 4 to 5.0 Torr and 300−445 K, respectively.

Intensity vs time profiles of mass selected ions were monitored using a PC-based multichannel scalar (MCS) data acquisition system, configured typically at 100 μs dwell time per channel over 250 channels. Additive accumulations of ion signals from 2000 electron gun beam pulses were used. Examples of both raw data as well as normalized time−intensity profiles for eq 21 are shown in Figures 3 and 4, respectively.

Equilibrium constants (K_{eq}) at different absolute temperatures for the various halide ion-trifluoro methyl halide clustering equilibria, eqs 21−23 are determined from eq 25 where

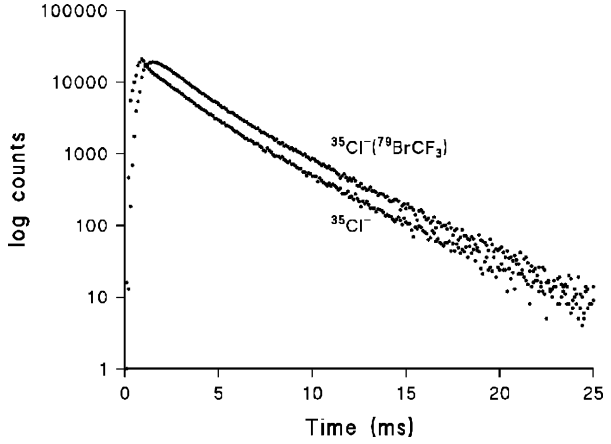

Figure 3. Experimental time−intensity profiles for the $^{35}Cl^- + CF_3{}^{79}Br \rightleftharpoons {}^{35}Cl^-(^{79}BrCF_3)$ clustering equilibrium at $P_{\text{ion source}} = 4.00$ Torr, $T_{\text{ion source}} = 322$ K, $P(CH_4) = 3.99$ Torr, $P(CF_3Br) = 0.01$ Torr, and $P(CCl_4) \ll 0.01$ Torr.

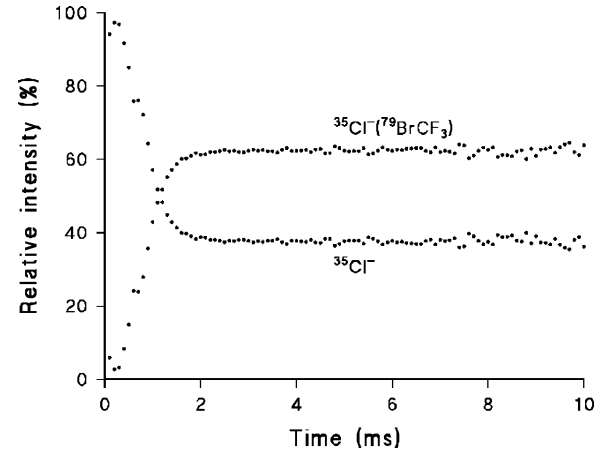

Figure 4. Normalized time−intensity profiles for the data shown in Figure 3.

$$K_{eq} = \frac{\text{Int}[X^-(CF_3Y)]}{\text{Int}[X^-]} \frac{P^o}{P_{CF_3Y,\text{source}}} \quad (25)$$

$\text{Int}[X^-(YCF_3)]/\text{Int}[X^-]$ is the ion intensity ratio of the $X^-(YCF_3)$ and X^- ions at equilibrium, $P°$ is the standard pressure (1 atm.), and $P_{CF_3Y,\text{source}}$ is the partial pressure (in atm) of the trifluoromethyl halide in the ion source.

From the equilibrium constants the standard Gibbs' free energy changes, ΔG, at different absolute temperatures, T, can be calculated from eq 26. By combining eqs 26 and 27 the van't Hoff equation, eq 28, can be obtained and from a plot of $\ln(K_{eq})$ vs $1/T$, both ΔH and ΔS for the clustering reaction can be obtained from the slope and intercept, respectively.

$$\Delta G = -RT \ln K_{eq} \quad (26)$$

$$\Delta G = \Delta H - T\Delta S° \quad (27)$$

$$\ln(K_{eq}) = \frac{\Delta S}{R} - \frac{\Delta H}{R}\frac{1}{T} \quad (28)$$

Equilibrium constants were calculated for various isotope pairs, e.g., $^{35}Cl^-/^{35}Cl^-(^{79}BrCF_3)$ and $^{35}Cl^-/^{35}Cl^-(^{81}BrCF_3)$ or $^{79}Br^-/^{79}Br^-(^{79}BrCF_3)$ and $^{79}Br^-/^{79}Br^-(^{81}BrCF_3)$. The observed equilibrium constants obtained for these isotope pairs must also be corrected for the fact that the partial pressure of CF_3Br introduced into the reservoir consists of 50% of $CF_3{}^{79}Br$ and 50% of $CF_3{}^{81}Br$. In addition, it must be recognized that the m/z value corresponding to $^{35}Cl^-(^{81}BrCF_3)$ also contains the $^{37}Cl^-(^{79}BrCF_3)$ isotope pair, and an appropriate correction was made.

Trifluoromethyl bromide and iodide were obtained from SCM Specialty Chemical Inc., methane was obtained from Praxair Ltd., carbon tetrachloride was obtained from J. T. Baker Chemical Co., and *n*-butyl bromide was obtained from Aldrich. All chemicals were used as received without further purification.

Computational Methods

All computations were performed using the *Gaussian 94*[95] and *Gaussian 98*[96] suites of programs. Geometries were optimized using the B3LYP method[97,98] in combination with the 6-311+G(d) (**a**) basis set for C, F, Cl, and Br,[99,100] and the LanL2DZ (**b**) basis set for I.[101] Normal mode vibrational frequencies and natural population analysis (NPA) charges were calculated at the same level of theory.[102] Single point energy computations were performed on the B3LYP level of theory in combination with the 6-311+G(3df) (**c**) basis set[103−106] on the B3LYP/**a** geometries. For some of the smaller systems investigated computations were performed using the MP2(full) method[107] in combination with basis set **a** for C, F, Cl, and Br, and modified LanL2DZ basis sets for I,[108] indicated here as LanL2DZ(spd) (**d**) and LanL2DZ(spdf) (**e**), or using the G3 and G3(MP2) methods.[109]

For the formation of $F^-(BrCF_3)$, $Cl^-(BrCF_3)$, and $Cl^-(CF_3Br)$ relaxed potential energy surface scans were performed at the B3LYP/**a** level of theory with the $F^-\cdots Br$, $Cl^-\cdots Br$, and $Cl^-\cdots C$ distances, respectively, as adjustable parameters, and optimizing all other bond distances, bond angles, and dihedral angles. An additional relaxed potential energy surface scan for $Cl^- + CF_3Cl$ through $Cl^-(CF_3Cl)$ to $[ClCF_3Cl]^{-‡}$ was performed as well.

Results and Discussion

1. Structures. The structures of CF_3Cl, CF_3Br, and CF_3I, as calculated at the B3LYP/**a** (CF_3Cl and CF_3Br) and B3LYP/[**a**/**b**] levels of theory, are summarized in Table 1, and compared with the corresponding experimental data. As can be seen, the agreement between theory and experiment[110−112] is good to excellent. Roszak et al. performed computations on the same molecules at the MP2 level in combination with larger basis sets, and the agreement between experiment and their results was in general slightly better than that obtained here.[113] The only significant trend observed for the three molecules is the elongation of the C−X bond length in going from X = Cl to I, which is mainly due to the increasing atomic size of the halide and the associated weaker bond. The C−F bond lengths and the X−C−F bond angles are remarkably constant for the three molecules. At this level of theory, there is excellent agreement for all three molecules with experimental dipole moments and normal mode vibrational frequencies (see below). For CF_3Cl, CF_3Br, and CF_3I dipole moments of 0.52, 0.66, and 1.08 D, respectively, were calculated, while, experimentally, corresponding values of 0.50, 0.65, and 1.05 D were determined.[114] Attachment of an electron into the LUMO of the trifluoromethyl halides to form the corresponding radical anions causes some significant structural changes. Elongation of the C−X bond by 0.864 and 0.813 Å for X = Cl and Br, respectively, is the most noticeable feature, which raises the question of whether $X^-(CF_3^•)$ might not be a better description for the $CF_3X^{-•}$ species. In Figure 5, the B3LYP/**a** structure of $CF_3Cl^{-•}$ is shown. The elongation of the C−X bond can best be explained by the fact that the LUMO is an antibonding σ-type orbital of a_1

TABLE 1: Computational B3LYP/a (b for Y = I) and Experimental Structural Data for CF_3Y and $CF_3Y^{-\bullet}$ (Y = Cl, Br, I) Species

	R(C−X)[a]		R(C−F)[a]		A(X−C−F)[b]	
structure	B3LYP/**a**	experiment	B3LYP/**a**	experiment	B3LYP/**a**	experiment
CF_3Cl	1.773	1.751 ± 0.005[d]	1.333	1.328 ± 0.002[d]	110.4	108.6 ± 0.4[d]
$CF_3Cl^{-\bullet}$	2.640		1.362		112.5	
CF_3Br	1.949	1.91 ± 0.03[e]	1.333	1.34 ± 0.02[e]	110.3	109.5 ± 2.0[e]
$CF_3Br^{-\bullet}$	2.762		1.363		112.3	
CF_3I[c]	2.162	2.135 ± 0.030[f]	1.336	1.340 ± 0.021[f]	110.6	108.4 ± 1.9[f]

[a] In Å. [b] In deg. [c] B3LYP/[**a**/**b.**] [d] From ref 110. [e] From ref 111. [f] From ref 112.

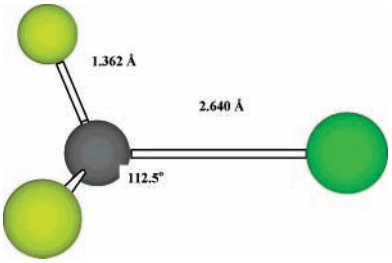

Figure 5. Optimized B3LYP/**a** structure of $CF_3Cl^{-\bullet}$.

TABLE 2: Computational B3LYP/a Structural Data for the Front-Side ($X^-(YCF_3)$) and Back-Side ($X^-(CF_3Y)$) Complexes (X = F, Cl, Br; Y = Cl, Br, I)

structure	R(C−Y)[a]	R(C−F)[a]	R(X⁻···Y)[a]	R(X⁻···C)[a]	A(Y−C−F)[b]
$F^-(BrCF_3)$	1.997	1.366	2.210		113.3
$F^-(CF_3Br)$	2.073	1.308		2.768	105.6
$Cl^-(ClCF_3)$	1.761	1.352	3.004		112.2
$Cl^-(CF_3Cl)$	1.829	1.319		3.770	108.2
$Cl^-(BrCF_3)$	1.974	1.356	2.875		112.5
$Cl^-(CF_3Br)$	2.013	1.317		3.724	108.0
$Cl^-(ICF_3)$[c]	2.238	1.361	2.967		112.9
$Cl^-(CF_3I)$[c]	2.258	1.317		3.714	108.1
$Br^-(ClCF_3)$	1.761	1.350	3.198		112.0
$Br^-(CF_3Cl)$	1.820	1.321		4.103	108.6
$Br^-(BrCF_3)$	1.976	1.354	3.047		112.4
$Br^-(CF_3Br)$	2.004	1.319		4.030	108.3
$Br^-(ICF_3)$[c]	2.243	1.359	3.122		112.8
$Br^-(CF_3I)$[c]	2.248	1.319		4.000	108.4

[a] In Å [b] In deg [c] B3LYP/[**a**/**b**].

symmetry almost entirely localized on the C−X bond and the extra electron is almost entirely localized on the halogen, X.[113] In addition, small increases in the C−F bond lengths and the X−C−F angle of around 0.03 Å and 2.0°, respectively are observed. Unfortunately, no experimental results for the three $CF_3X^{-\bullet}$ species are available. Compared to the analogous results obtained by Roszak et al. for CF_3X and $CF_3X^{-\bullet}$ (X = Cl, Br) the C−X bond lengths reported here are slightly longer,[113] by ∼0.03 Å for CF_3X and by ∼0.06 Å for $CF_3X^{-\bullet}$.

As noted above, complex formation between X^- and CF_3Y can give rise to two possible ion−molecule complexes arising from front-side and back-side attack, respectively, eqs 29 and 30.

$$X^- + CF_3Y \rightleftharpoons X^-(YCF_3) \quad (29)$$

$$X^- + CF_3Y \rightleftharpoons X^-(CF_3Y) \quad (30)$$

In Table 2, the essential features of the structures of the front-side and back-side attack complexes of F^- with CF_3Br, and both Cl^- and Br^- with CF_3Cl, CF_3Br, and CF_3I are summarized. In each of the front-side attack complex species, $X^-(YCF_3)$, X^- interacts with the positive end of the dipole moment in CF_3Y such that each species adopts a linear arrangement of the C, Y, and X atoms. In the back-side attack complex species, $X^-(CF_3Y)$, on the other hand, X^- experiences some electrostatic repulsion from the three fluorine atoms in CF_3Y, which each bear a partial negative charge. This is most evident from the substantially longer X⁻···C distances found in CF_3Y complexes relative to those in the analogous CH_3Y complexes. The structural data in Table 2 also show how the structural features in both the $X^-(YCF_3)$ and $X^-(CF_3Y)$ complexes are different, not just relative to each other but also relative to the isolated CF_3Y. In general, the C−Y bond in both the $X^-(YCF_3)$ and $X^-(CF_3Y)$ complexes is longer than that in CF_3Y, with the former shorter than the latter. The sole exceptions to this trend are the Cl^- and Br^- front-side attack complexes of CF_3Cl where the C−Cl bond length in the CF_3Cl moiety is about 0.01 Å shorter in each case than that in CF_3Cl itself. For the C−F bonds in $X^-(YCF_3)$, a small increase in C−F bond length is observed relative to CF_3Y, while for $X^-(CF_3Y)$ a small decrease takes place. The X⁻···YCF_3 distances in the $X^-(YCF_3)$ complexes show a nonmonotonic trend. For X = Cl and Br, and constant Y, R(X⁻···Y) increases from X = Cl to Br for all Y's, as expected due to the increasing ionic radius and the associated more diffuse nature of the larger halide. For either X = Cl or Br and Y = Cl, Br, and I, R(X⁻···Y) decreases as Y proceeds from Cl to Br, while it increases as Y goes from Br to I. This is likely due to the competing effects of increasing halogen size vs increasing dipole moment and polarizability. In the cases of $Cl^-(BrCF_3)$ and $Br^-(BrCF_3)$ the interhalogen distances are within 0.05 Å of those in $ClBr^{-\bullet}$ or $Br_2^{-\bullet}$, respectively. However for $Cl^-(ClCF_3)$ and $Br^-(ClCF_3)$ the interhalogen distances are 0.23 and 0.33 Å longer, respectively than those in $Cl_2^{-\bullet}$ or $ClBr^{-\bullet}$. For the $X^-(CF_3Y)$ complexes, different and more logical trends are observed. This can be ascribed simply as being the result of the competing effects of increasing bond strength in the adduct, counterbalanced by the increasing size of the halogen. In going from Y = Cl to Br to I in all $X^-(CF_3Y)$, the R(X⁻···C) simply decreases. Finally, in the $X^-(YCF_3)$ complexes, the Y−C−F angles are larger than in CF_3Y, while in the $X^-(CF_3Y)$ complexes they are somewhat smaller. Similar observations have been made for CH_3X, $X^-(CH_3X)$, and $X^-(XCH_3)$ (X = Br, I) at the MP2(fc)/[6-31+G(d)/LanL2DZ-(spd)] level of theory.[37,39] For both $X^-(CH_3X)$ and $X^-(XCH_3)$ small increases in R(C−X) relative to CH_3X take place. For R(C−H) a small decrease relative to CH_3X takes place in $X^-(CH_3X)$, while a small increase takes place in $X^-(XCH_3)$. Last, in $X^-(CH_3X)$ a small decrease in the X−C−H angle takes place, while in $X^-(XCH_3)$ the angles do not change perceptibly relative to free CH_3X.

For the back- and front-side attack mechanisms, separate transition states are also possible, indicated by $[XCF_3Y]^{-\ddagger}$ and $[CF_3XY]^{-\ddagger}$, respectively. In Table 3, the results for the four $[XCF_3Y]^{-\ddagger}$ transition states are summarized, while in Figure 6 the structures of $[FCF_3Br]^{-\ddagger}$ and $[ClCF_3Cl]^{-\ddagger}$ are shown. It is noteworthy that the C···Br distances in $[FCF_3Br]^{-\ddagger}$ and $[ClCF_3Br]^{-\ddagger}$ are shorter than that in $[BrCF_3Br]^{-\ddagger}$ indicating early

TABLE 3: Computational B3LYP/a Structural Data for the $[XCF_3Y]^{-‡}$ Transition States (X, Y = F, Cl, Br)

structure	$R(X\cdots C)^a$	$R(C\cdots Y)^a$	$R(C-F)^a$	$A(X\cdots C-F)^b$	$A(F-C-F)^b$
$[FCF_3Br]^{-‡}$	2.244	2.293	1.298	81.8	120.0
$[ClCF_3Cl]^{-‡}$	2.488	2.488	1.284	90.0	120.0
$[ClCF_3Br]^{-‡}$	2.536	2.630	1.283	89.1	120.0
$[BrCF_3Br]^{-‡}$	2.667	2.667	1.283	90.0	120.0

[a] In Å. [b] In deg.

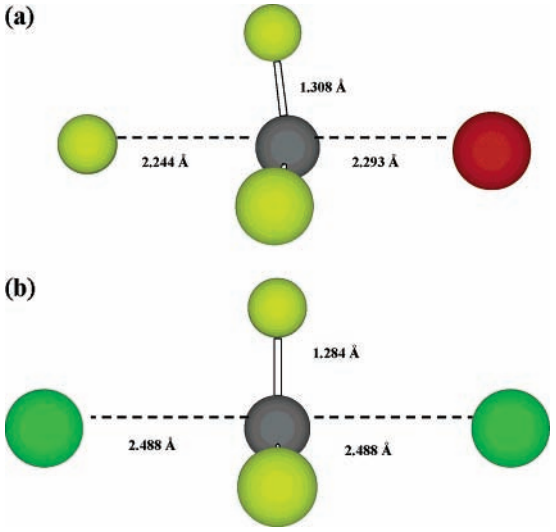

Figure 6. (a) Optimized B3LYP/**a** structure of $[FCF_3Br]^{-‡}$. (b) Optimized B3LYP/**a** structure of $[ClCF_3Cl]^{-‡}$.

TABLE 4: Computational B3LYP/a Structural Data for the $[CF_3XY]^{-‡}$ Transition States (X, Y = Cl, Br)

	structure		
	$[CF_3Cl_2]^-$	$[CF_3ClBr]^-$	$[CF_3Br_2]^-$
$R(C\cdots X)^a$	2.410	2.437	2.638
$R(C\cdots Y)^a$	2.410	2.618	2.646
$R(X\cdots Y)^a$	3.151	3.317	3.487
$R(C-F_A)^a$	1.325	1.325	1.326
$R(C-F_{BX})^a$	1.360	1.325	1.353
$R(C-F_{BY})^a$	1.360	1.360	1.353
$A(X\cdots C\cdots Y)^b$	81.6	81.9	82.6
$A(X\cdots C-F_A)^b$	97.6	95.3	97.3
$A(Y\cdots C-F_A)^b$	97.6	100.2	97.6
$A(X\cdots C-F_{BX})^b$	82.7	83.1	81.7
$A(Y\cdots C-F_{BY})^b$	82.7	81.1	81.2

[a] In Å. [b] In deg.

transition states in the first two cases. Similarly, the C···Cl distance in $[ClCF_3Cl]^{-‡}$ is shorter than that in $[ClCF_3Br]^{-‡}$. The C−F distances in all cases are slightly shorter than in the $X^-(CF_3Y)$ complexes. Compared to the Cl···C distance of 2.371 Å in $[ClCH_3Cl]^{-‡}$, as calculated at the B3LYP/6-311+G(d,p) level of theory, the substitution of hydrogen atoms by fluorine atoms increases this distance by 0.117 Å.[40]

The $[CF_3XY]^{-‡}$ front-side attack transition states calculated for this work show features similar to $[CH_3X_2]^{-‡}$ obtained by Glukhovtsev et al. [39] The structural data for $[CF_3Cl_2]^{-‡}$, $[CF_3ClBr]^{-‡}$, and $[CF_3Br_2]^{-‡}$ are shown in Table 4 based on the atom definitions given in Figure 7. As an example, the structure of $[CF_3Cl_2]^{-‡}$ is shown in Figure 8. For $[CF_3Cl_2]^{-‡}$ the C···Cl distances are 0.078 Å shorter than in $[ClCF_3Cl]^{-‡}$, while in $[CF_3Br_2]^{-‡}$ the C···Br distance is, on average, 0.025 Å shorter relative to $[BrCF_3Br]^{-‡}$. The X···Y distance increases as expected from $[CF_3Cl_2]^{-‡}$ to $[CF_3Br_2]^{-‡}$, but in all three structures it is approximately 0.40−0.50 Å longer than in the isolated $XY^{-•}$ species. The C−F distances are slightly longer

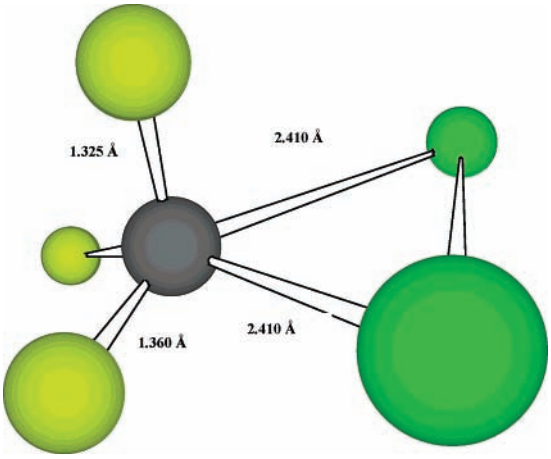

Figure 7. Optimized B3LYP/**a** structure of $[CF_3Cl_2]^{-‡}$.

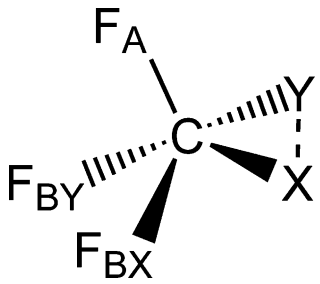

Figure 8. Atom labeling in the $[CF_3XY]^{-‡}$ transition states.

TABLE 5: Computational B3LYP/a and MP2(full)/a (b for I), and Experimental Structural Data for XY and $XY^{-•}$ (X, Y = Cl, Br, I)

	$R(X-Y)^a$		
structure	B3LYP/**a**	MP2(full)/**a**	experiment
Cl_2	2.053	2.024	1.988[c]
$Cl_2^{-•}$	2.755	2.650	
ClBr	2.191	2.164	
$ClBr^{-•}$	2.865	2.747	
Br_2	2.330	2.303	2.283[c]
$Br_2^{-•}$	2.990	2.869	
I_2^b	2.710	2.692	2.666[c]
$I_2^{-•b}$	3.381	3.282	

[a] In Å. [b] LanL2DZ(spd). [c] From ref 115.

than in the $[XCF_3Y]^{-‡}$ transition states, with the $C-F_A$ bond length shorter than the $C-F_B$ bond length. There are small variations in the various bond angles, but these are sufficiently small as to not influence the discussion here. Replacing one of the fluorine atoms by a chlorine atom produces some effect as seen from the $[BrCF_2Cl_2]^{-‡}$ and $[CF_2Cl_2Br]^{-‡}$ transition state structures relative to $[ClCF_3Br]^{-‡}$ and $[CF_3ClBr]^{-‡}$, respectively. In both structures there are increases in the C···X, C···Y, X···Y, and C−F bond lengths. In $[CF_2Cl_2Br]^{-‡}$ the C−Cl bond length is longer than that in $[BrCF_2Cl_2]^{-‡}$ (1.777 and 1.705 Å, respectively). Compared to the structures of $[CH_3Cl_2]^{-‡}$ and $[CH_3Br_2]^{-‡}$ at the MP2/6-31+G(d) and MP2/[6-31+G(d)/ECP] level of theory,[39] respectively, the X···X distances are actually longer than in $[CF_3Cl_2]^{-‡}$ and $[CF_3Br_2]^{-‡}$ from this work. Loosely bound e;ectrostatic complexes of CF_3 and $XY^{-•}$ were also searched for, but without success. All such structures attempted collapsed to one or the other of the front-side attack complexes.

Finally, in Table 5, a summary is given of the B3LYP/**a**, MP2(full)/**a** (**d** for X, Y = I), for the XY and $XY^{-•}$ species (X, Y = Cl, Br, I). As expected there is an increase in the X−Y

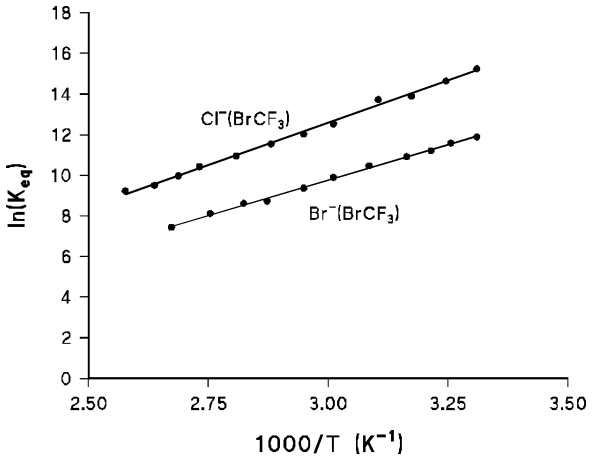

Figure 9. Van't Hoff plots for the halide ion-trifluoro methyl halide clustering equilibria: $X^- + CF_3Br \rightleftharpoons X^-(BrCF_3)$ (X = Cl, Br).

bond distance in going from XY and $XY^{-\bullet}$. In general, the agreement between the MP2 results and experiment [115] is closer than that for the B3LYP data, but the B3LYP values may still be considered adequate to be used for the purposes of the arguments made in the present discussion.

2. Experimental and Computational Thermochemistry. For the complex formation equilibria of the halide ion-trifluoromethyl halides, eqs 29 and 30, no experimental thermochemistry is available in the literature. In Figure 9, the experimental van't Hoff plots for the formation of $Cl^-(BrCF_3)$ and $Br^-(BrCF_3)$ are shown.

A summary of the available experimental and computational thermochemistry is given in Table 6 for the formation of the various $X^-(YCF_3)$ and $X^-(CF_3Y)$ complexes. It can be seen that the agreement between experimental and computational results is good to excellent. With the exceptions of the formation of $F^-(BrCF_3)$, $Br^-(ICF_3)$, and perhaps $Cl^-(ClCF_3)$, no other systems would be accessible experimentally due to the very small binding energies involved. For all back-side attack complexes, $X^-(CF_3Y)$, the $\Delta G_{298}°$ values are positive, so these complexes may only exist at very low temperatures. Measuring the experimental thermochemistry for the formation of $F^-(BrCF_3)$ would only be possible at temperatures higher than 500 K and at these temperatures competition from the displacement reaction may well render the clustering reaction unobservable. The $\Delta H°$ value for eq 23 was determined from the $\Delta G°$ values at 432 and 446 K and the $\Delta S°_{298}$ value from the DFT computations. With increasing ion source temperature, the total ion intensity dropped quickly and had completely disappeared at 460 K, most probably due to plugging of the ion exit aperture by HI, or possibly I_2, formed by electron radiolysis of CF_3I. The close agreement between experiment and theory gives confidence that the chosen level of theory is suitable for these kinds of systems.

In addition to nucleophilic displacement and complex formation, formation of XY and $XY^{-\bullet}$ by Y^+ and $Y^\bullet$ abstraction, respectively, are also possible processes that should be considered while exploring the potential energy surfaces for eqs 31 and 32 in the reaction between X^- and CF_3Y.

$$X^- + CF_3Y \rightarrow CF_3^- + XY \qquad (31)$$

$$X^- + CF_3Y \rightarrow XY^{-\bullet} + CF_3^\bullet \qquad (32)$$

In Table 7, the computational $\Delta H°_{298}$ values for these additional possible reaction channels are summarized, as well as the experimental data where available. The latter values are derived from the thermochemical data given in Table 8.[116] With the exception of the reactions involving radicals and/or radical anions as products, in general the agreement is very good to excellent. It is interesting to note that the electron affinity (EA) of ClBr has never been determined. In Table 9, the calculated electron affinities (in eV) as well as the bond dissociation energies (BDE) (in kcal mol^{-1}) of the various species involved in the different reactions have been summarized. Results from B3LYP, MP2, G3, and G3(MP2) calculations are given, as well as corresponding experimental data. For the few systems investigated, calculations at the G3 and G3(MP2) levels seem to perform very well. Except for the EA of $CF_3^\bullet$ and the BDE of ClBr, the B3LYP/**c**//B3LYP/**a** method chosen performs less accurately than the MP2(full)/**a** computations. Use of different basis sets or use of composite methods such G2 or G3 may be more accurate, but they also more computationally demanding and consequently more expensive.

In Table 10, the calculated activation enthalpies, $\Delta H^‡_{298}$, for the front- and back-side attack mechanisms, eqs 33 and 34, relative to the reactants are summarized, including the only experimental result available.[88]

$$X^- + CF_3Y \rightarrow [CF_3XY]^{-‡} \qquad (33)$$

$$X^- + CF_3Y \rightarrow [XCF_3Y]^{-‡} \qquad (34)$$

The suggestion of Morris and Viggiano, that eq 18 proceeds through the classical Walden inversion, a back-side attack mechanism, had already seemed to be a very reasonable conclusion based on all of their observations.[91] On the other hand, arguments that the three fluorine atoms might shield attack at the carbon also seem reasonable a priori. This assumption was seemingly supported by the fact that Staneke et al. failed to observe formation of Br^- from the reaction between OH^- and CF_3Br.[93] Results from the present work confirm that the conclusion of Morris and Viggiano was indeed correct, since $\Delta H^‡_{298}$ for $[FCF_3Br]^{-‡}$ is -6.3 kcal mol^{-1}. Ho and McMahon had suggested that eq 15 could proceed through a front-side attack transition state $[CF_3Cl_2Br]^{-‡}$.[88] Comparison of the transition state energetics for front- (47.2 kcal mol^{-1}) and back-side (24.6 kcal mol^{-1}) attack mechanisms relative to the experimental threshold energy of 21.0 ± 1.2 kcal mol^{-1}, shows clearly that this reaction also likely proceeds through a back-side attack mechanism. Since $\Delta G°$ for the formation of $X^-(CF_3Y)$ is greater than zero at room temperature, it is highly probable that the lifetime of any complex formed would be exceedingly short and it would be likely that the reaction could only proceed via a so-called direct mechanism. This actually then more closely resembles the mechanism of a condensed phase S_N2 reaction, eq 35.

$$X^- + CF_3Y \rightarrow [XCF_3Y]^{-‡} \rightarrow XCF_3 + Y^- \qquad (35)$$

In Table 10, all transition states for back-side attack are lower in energy than for the front-side attack mechanism. Unfortunately it was not possible to test the computations by performing experiments similar to those of Hop and McMahon using FT-ICR threshold measurements. Guided ion beam (GIB) experiments such as those carried out by Ervin and co-workers on a number of more conventional S_N2 systems would be extremely valuable,[15] since that technique is much more suited to the measurement of accurate cross sections and threshold energies. The higher energy transition state $[CF_3XY]^{-‡}$ might also be accessed experimentally in such experiments. Close inspection of the NPA charges (see below) indicates that it

TABLE 6: Experimental PHPMS and Computational B3LYP/c//B3LYP/a Thermochemical Data for the Formation of $X^-(YCF_3)$ and $X^-(CF_3Y)$ Complexes (X = F, Cl, Br; Y = Cl, Br, I)

clustering equilibrium	$\Delta H°_{298}$ [a] B3LYP/**c**//B3LYP/**a**	$\Delta H°$ [a] PHPMS	$\Delta S°_{298}$ [b] B3LYP/**a**	$\Delta S°$ [b] PHPMS
$F^- + CF_3Br \rightleftharpoons F^-(BrCF_3)$	−30.9		−24.8	
$F^- + CF_3Br \rightleftharpoons F^-(CF_3Br)$	−8.2		−22.1	
$Cl^- + CF_3Cl \rightleftharpoons Cl^-(ClCF_3)$	−9.8		−21.2	
$Cl^- + CF_3Cl \rightleftharpoons Cl^-(CF_3Cl)$	−2.3		−17.3	
$Cl^- + CF_3Br \rightleftharpoons Cl^-(BrCF_3)$	−14.9	−16.5 ± 0.2	−22.3	−24.5 ± 1.0
$Cl^- + CF_3Br \rightleftharpoons Cl^-(CF_3Br)$	−2.4		−17.8	
$Cl^- + CF_3I \rightleftharpoons Cl^-(ICF_3)$ [c]	−21.5	−23.6 ± 0.2	−22.3	
$Cl^- + CF_3I \rightleftharpoons Cl^-(CF_3I)$ [c]	−2.6		−17.2	
$Br^- + CF_3Cl \rightleftharpoons Br^-(ClCF_3)$	−8.0		−20.5	
$Br^- + CF_3Cl \rightleftharpoons Br^-(CF_3Cl)$	−1.4		−15.5	
$Br^- + CF_3Br \rightleftharpoons Br^-(BrCF_3)$	−12.5	−13.9 ± 0.2	−21.8	−22.2 ± 1.0
$Br^- + CF_3Br \rightleftharpoons Br^-(CF_3Br)$	−1.2		−15.7	
$Br^- + CF_3I \rightleftharpoons Br^-(ICF_3)$ [c]	−18.7		−21.9	
$Br^- + CF_3I \rightleftharpoons Br^-(CF_3I)$ [c]	−1.7		−15.7	

[a] In kcal mol^{-1}. [b] In cal mol^{-1} K^{-1}. [c] B3LYP/[**b**/**c**]//B3LYP/[**a**/**c**].

TABLE 7: Computational B3LYP/c//B3LYP/a and Experimental Thermochemical Data for the Reactions: $X^- + CF_3Y \rightarrow Y^- + CF_3X$, $XY^{-\bullet} + CF_3^{-\bullet}$, $CF_3Y^{-\bullet} + X^\bullet$, and $CF_3^- + XY$ (X = F, Cl, Br; Y = Cl, Br)

reaction	$\Delta H°_{298}$ [a] B3LYP/**b**//B3LYP/**a**	$\Delta H°$ [a] experiment[b]
$F^- + CF_3Br \rightarrow Br^- + CF_4$	−59.6	−59.4
$Cl^- + CF_3Cl \rightarrow Cl^- + CF_3Cl$	0.0	0.0
$Cl^- + CF_3Cl \rightarrow Cl_2^{-\bullet} + CF_3^\bullet$	+45.2	+57.4
$Cl^- + CF_3Cl \rightarrow CF_3Cl^{-\bullet} + Cl^\bullet$	+67.6	NA
$Cl^- + CF_3Cl \rightarrow CF_3^- + Cl_2$	+69.6	+70.2
$Cl^- + CF_3Br \rightarrow Br^- + CF_3Cl$	−10.8	−10.5
$Cl^- + CF_3Br \rightarrow ClBr^{-\bullet} + CF_3^\bullet$	+33.7	NA
$Cl^- + CF_3Br \rightarrow CF_3Br^{-\bullet} + Cl^\bullet$	+57.8	+63.2
$Cl^- + CF_3Br \rightarrow CF_3^- + ClBr$	+58.1	+59.6
$Br^- + CF_3Cl \rightarrow Cl^- + CF_3Br$	+10.8	+10.5
$Br^- + CF_3Cl \rightarrow ClBr^{-\bullet} + CF_3^\bullet$	+44.4	NA
$Br^- + CF_3Cl \rightarrow CF_3Cl^{-\bullet} + Br^\bullet$	+64.8	NA
$Br^- + CF_3Cl \rightarrow CF_3^- + ClBr$	+68.9	+70.1
$Br^- + CF_3Br \rightarrow Br^- + CF_3Br$	0.0	0.0
$Br^- + CF_3Br \rightarrow Br_2^{-\bullet} + CF_3^\bullet$	+33.6	+43.3
$Br^- + CF_3Br \rightarrow CF_3Br^{-\bullet} + Br^\bullet$	+54.9	+57.4
$Br^- + CF_3Br \rightarrow CF_3^- + Br_2$	+58.5	+59.9

[a] kcal mol^{-1}. [b] From ref 116.

TABLE 8: Experimental Standard Heats of Formation, $\Delta_f H°$, of Various Neutrals and (Radical) Anions

structure	$\Delta_f H°$ [a]	structure	$\Delta_f H°$ [a]
$F^\bullet$	+19.0	F^-	−59.4
$Cl^\bullet$	+29.0	Cl^-	−54.4
$Br^\bullet$	+26.7	Br^-	−50.9 ± 0.2
$I^\bullet$	+25.5	I^-	−45.1
$CF_3^\bullet$	−112.4	CF_3^-	−154.7 ± 4.4
Cl_2	0.0	$Cl_2^{-\bullet}$	−55.3 ± 4.6
ClBr	+3.5	$ClBr^{-\bullet}$	NA
Br_2	+7.4	$Br_2^{-\bullet}$	−50.3
I_2	+14.9	$I_2^{-\bullet}$	−43.3 ± 0.1
CF_4	−223.0	$CF_4^{-\bullet}$	NA
CF_3Cl	−169.2	$CF_3Cl^{-\bullet}$	NA
CF_3Br	−155.1	$CF_3Br^{-\bullet}$	−176.3 ± 4.6

[a] In kcal mol^{-1}. [b] From ref 116.

closely resembles a $[CF_3^\bullet XY^{-\bullet}]^\ddagger$ species. Monitoring the cross section for formation of $XY^{-\bullet}$ as a function of the center-of-mass kinetic energy of X^- might then give information on the energy of $[CF_3XY]^{-\ddagger}$ relative to the reactants X^- and CF_3Y. It should be noted however that Ervin and co-workers report that such experiments often yield excess thresholds due to angular momentum barriers and the inefficiency of collisional activation in promoting these reactions.[25b,c]

In Figures 10−12, all computational B3LYP/**c**//B3LYP/**a** $\Delta H°_{298}$ and $\Delta H^\ddagger_{298}$ values for the various reactions are summarized in schematic potential energy diagrams. Even though the substitution of hydrogen atoms by fluorine atoms does not reverse the order of back- and front-side attack mechanisms in gas-phase S_N2 reactions, the difference between the two transition states has been reduced considerably. This is mainly due to the large increase in the $\Delta H^\ddagger_{298}$ values for back-side attack and a small decrease in the ΔH_{298} values for front-side attack.

The relationship between kinetics and thermodynamics plays an important role in chemistry. Marcus has derived an expression, the Marcus equation, which originally related the activation energy to the thermochemistry of electron-transfer reactions in solution, eq 36.[116] Brauman and co-workers[117−120] have subsequently shown that this relationship can be applied similarly to transfer of other moieties in the gas-phase such as occurs in the gas-phase S_N2

$$\Delta E^\ddagger = \Delta E_0^\ddagger + \frac{\Delta E}{2} + \frac{(\Delta E)^2}{16\Delta E_0^\ddagger} \qquad (36)$$

reaction. In Figure 13, a typical gas-phase S_N2 double well potential energy diagram is shown indicating the definitions of $\Delta E^\ddagger$ and ΔE in eq 37. $\Delta E_0^\ddagger$ can be determined from the Marcus additivity postulate, eq 37.[116]

$$\Delta E_0^\ddagger = \frac{1}{2}(\Delta E_{XX}^\ddagger + \Delta E_{YY}^\ddagger) \qquad (37)$$

In eq 37 $\Delta E_{XX}^\ddagger$ and $\Delta E_{YY}^\ddagger$ are the intrinsic kinetic contributions to the activation energy for the identity gas-phase S_N2 reactions, eqs 38 and 39.

$$X^- + CH_3X \rightarrow X^- + CH_3X \qquad (38)$$

$$Y^- + CH_3Y \rightarrow Y^- + CH_3Y \qquad (39)$$

Brauman's group has shown both experimentally and using RRKM modeling that eq 36 applies to a large variety of nonidentity gas-phase S_N2 reactions.[9,117−120] This was supported theoretically by Wolfe et al. from ab initio computations,[121,122] as well as by Shaik and Pross.[123]

Despite the limited amount of data available, it is of interest to question if the high barrier S_N2 reactions described here might also follow eq 36. From the B3LYP/**c**//B3LYP/**a** computations it can be determined that for the back-side attack mechanism,

TABLE 9: Computational B3LYP/c//B3LYP/a, MP2/a, G3, and G3(MP2), and Experimental Electron Affinities and Bond Dissociation Energies of Various (Radical) Neutrals and Radical Anions

	$\Delta H^\circ_{298}{}^{a,b}$				$\Delta H^{\circ a,b}$
reaction	B3LYP/**c**//B3LYP/**a**	MP2(full)/**a**	G3	G3(MP2)	experiment[d]
$Cl^\bullet + e^- \rightarrow Cl^-$	−3.68	−3.16	−3.61	−3.67	−3.61
$Cl_2 + e^- \rightarrow Cl_2^{-\bullet}$	−2.84	−2.47	−2.45	−2.47	−2.40
$ClBr + e^- \rightarrow ClBr^{-\bullet}$	−2.85	−2.46			NA
$Br^\bullet + e^- \rightarrow Br^-$	−3.56	−3.13			−3.36
$Br_2 + e^- \rightarrow Br_2^{-\bullet}$	−2.87	−2.56			−2.55
$I_2 + e^- \rightarrow I_2^{-\bullet}$[c]	−2.97	−2.53			−2.52
$CF_3^\bullet + e^- \rightarrow CF_3^-$	−1.79	−1.52			−1.83[e]
$CF_3Cl + e^- \rightarrow CF_3Cl^{-\bullet}$	−0.75			−0.86	NA
$CF_3Br + e^- \rightarrow CF_3Br^{-\bullet}$	−1.18				−0.92
$Cl_2 \rightarrow 2Cl^\bullet$	+54.8	+42.1	+56.8	+57.5	+58.0
$ClBr \rightarrow Cl^\bullet + Br^\bullet$	+52.6	+42.3			+52.2
$Br_2 \rightarrow 2Br^\bullet$	+49.4	+41.3			+46.0
$Cl_2^{-\bullet} \rightarrow Cl^- + Cl^\bullet$	+35.4	+26.0	+30.3	+29.7	+29.9
$ClBr^{-\bullet} \rightarrow Cl^- + Br^\bullet$	+33.4	+26.1			NA
$ClBr^{-\bullet} \rightarrow Br^- + Cl^\bullet$	+36.2	+26.8			NA
$Br_2^{-\bullet} \rightarrow Br^- + Br^\bullet$	+33.5	+26.6			+26.1

[a] In eV. [b] In kcal mol^{-1}. [c] LanL2DZ(spd) basis set for I. [d] From ref 116. [e] From ref 133.

TABLE 10: Computational B3LYP/c//B3LYP/a Thermochemistry for the Reactions: $X^- + CF_3Y \rightarrow [XCF_3Y]^{-\ddagger}$ or $[CF_3XY]^{-\ddagger}$ (X = F, Cl, Br; Y = Cl, Br)

reaction	$\Delta H^\ddagger_{298}{}^a$ for B3LYP/b//B3LYP/a	$E_a{}^a$ for experiment
$F^- + CF_3Br \rightarrow [FCF_3Br]^{-\ddagger}$	−6.3	
$Cl^- + CF_3Cl \rightarrow [ClCF_3Cl]^{-\ddagger}$	+20.7	
$Cl^- + CF_3Cl \rightarrow [CF_3Cl_2]^{-\ddagger}$	+43.9	
$Cl^- + CF_3Br \rightarrow [ClCF_3Br]^{-\ddagger}$	+15.5	
$Cl^- + CF_3Br \rightarrow [CF_3ClBr]^{-\ddagger}$	+36.3	
$Br^- + CF_3Cl \rightarrow [BrCF_3Cl]^{-\ddagger}$	+26.2	
$Br^- + CF_3Cl \rightarrow [CF_3ClBr]^{-\ddagger}$	+47.1	
$Br^- + CF_3Br \rightarrow [BrCF_3Br]^{-\ddagger}$	+20.8	
$Br^- + CF_3Br \rightarrow [CF_3Br_2]^{-\ddagger}$	+39.9	
$Br^- + CF_2Cl_2 \rightarrow [BrCF_2Cl_2]^{-\ddagger}$	+24.6	+21.0 ± 1.2[b]
$Br^- + CF_2Cl_2 \rightarrow [CF_2Cl_2Br]^{-\ddagger}$	+47.2	

[a] In kcal mol^{-1}. [b] From ref 88.

$\Delta E^\ddagger_{ClCl}$ and $\Delta E^\ddagger_{BrBr}$ are +23.0 and +22.0 kcal mol^{-1}, respectively, giving a $\Delta E^\ddagger_0$ value of +22.5 kcal mol^{-1}. ΔE_{ClBr} has a value of −9.8 kcal mol^{-1}, which results in a $\Delta E^\ddagger$ value of +17.9 kcal mol^{-1} from eq 36. By using the B3LYP/**c**// B3LYP/**a** results an identical value is obtained. Similarly, a consideration of the front-side attack mechanism yields excellent agreement. $\Delta E^\ddagger_{ClCl}$ and $\Delta E^\ddagger_{BrBr}$ are +53.7 and +52.4 kcal mol^{-1}, respectively, giving a $\Delta E^\ddagger_0$ value of +53.0 kcal mol^{-1}. $\Delta E^\ddagger_{BrBr}$ has a value of −3.9 kcal mol^{-1}, which results in a $\Delta E^\ddagger$ value of +51.1 kcal mol^{-1} from eq 36. By using the B3LYP/**c**// B3LYP/**a** results an almost identical value of 51.2 kcal mol^{-1} is obtained. Thus, the simple Marcus equation is seen to be a reliable treatment of both possible mechanisms for the S_N2 reactions of trifluoromethyl halides.

Finally, it can be noted that, at the G3(MP2) level of theory, the $\Delta H_f{}^\circ_{298}$ values of CF_3Cl and $CF_3Cl^{-\bullet}$ have been calculated to be −173.1 and −193.0 kcal mol^{-1}, respectively. The first of these is in reasonably good agreement with the experimental value of −169.2 kcal mol^{-1}.[124]

3. Normal Mode Vibrational Frequencies. It was shown above that the B3LYP/**a** level of theory ([**a**/**b**] for CF_3I) is able to generate structures and dipole moments of the CF_3X molecules that are in good agreement with experimental data. This agreement was a determining factor in the use of this level of theory for the subsequent computations on the ion−molecule complexes and transition states. In Table 11 an overview is given of the calculated and experimental normal mode vibrational frequencies of CF_3Cl, CF_3Br, and CF_3I.[126] The excellent agreement confirms once again that the B3LYP/**a** level of theory appears to be an acceptable choice. As noted above, the $[CF_3XY]^{-\ddagger}$ transition state seems to closely resemble a $[CF_3^\bullet XY^{-\bullet}]^\ddagger$ complex, and it may be the transition state for a high kinetic energy S_N2 reaction, eq 40, as well as that for $XY^{-\bullet}$ formation, eq 41. In the $[CF_3XY]^{-\ddagger}$ transition state, the imaginary frequency corresponds to a combined

$$X^- + CF_3Y \rightarrow [CF_3XY]^{-\ddagger} \rightarrow Y^- + CF_3X \qquad (40)$$

$$X^- + CF_3Y \rightarrow [CF_3XY]^{-\ddagger} \rightarrow XY^{-\bullet} + CF_3^\bullet \qquad (41)$$

C ← X and C → Y motion. In addition, there is an X↔Y motion, and the corresponding frequency is very close to the frequency in "free" $XY^{-\bullet}$. In $[CF_3Cl_2]^{-\ddagger}$, $[CF_3ClBr]^{-\ddagger}$, and $[CF_3Br_2]^{-\ddagger}$ these frequencies are 179, 140, and 100 cm^{-1}, respectively, while in $Cl_2^{-\bullet}$, $ClBr^{-\bullet}$, and $Br_2^{-\bullet}$ they are 198, 163, and 118 cm^{-1}, respectively.

The imaginary frequency in the $[XCF_3Y]^{-\ddagger}$ transition state is larger in magnitude than that in the isomeric $[CF_3XY]^{-\ddagger}$ transition state. For all three systems investigated it is consistently around 510*i*, while for the front-side attack transition state it decreases from 210*i* to 185*i* to 163*i*. Examination of the motion of the imaginary frequency in the $[XCF_3Y]^{-\ddagger}$ transition state shows that it is an umbrella-like inversion of the CF_3 group. This would also explain the increased barrier height, relative to CH_3. Substitution of one of the fluorine atoms by a chlorine atom decreases the imaginary frequencies in $[ClCF_2ClBr]^{-\ddagger}$ and $[CF_2Cl_2Br]^{-\ddagger}$ to 428*i* and 176*i*, respectively.

4. Natural Population Analysis (NPA) Charges. In proceeding from CF_3Cl to CF_3I the NPA charge on the halogen atom increases from 0.00*e* to +0.15*e*. As expected, the fluorine atoms bear considerable negative charge, with each around −0.33*e*, while the carbon atom is positively charged, ranging from +0.88*e* in CF_3I to +1.00*e* in CF_3Cl. This thus gives an indication of the preference for X^- to interact with Y in CF_3Y, but also shows that back-side attack on carbon is still feasible. Upon formation of the $X^-(YCF_3)$ complex some charge redistribution takes place. First, partial charge transfer from X^- to CF_3Y takes place, ranging from +0.08*e* in $Cl^-(ClCF_3)$ to +0.22*e* in $Br^-(ICF_3)$. The NPA charge on Y becomes more positive, while on carbon it becomes generally somewhat less positive, dropping to around +0.90*e*. All fluorine atoms become more negatively charged to around −0.39*e*. Formation of the

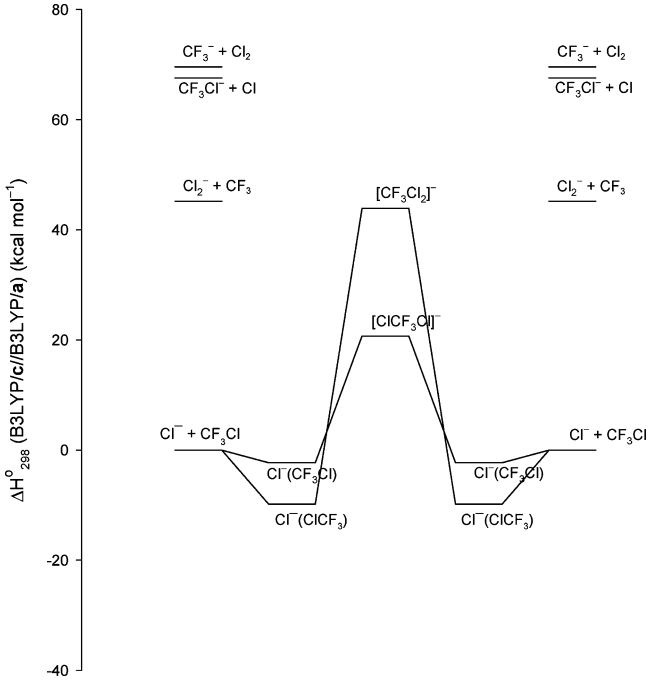

Figure 10. Schematic B3LYP/**c**//B3LYP/**a** potential energy profile for the various $Cl^- + CF_3Cl$ reactions.

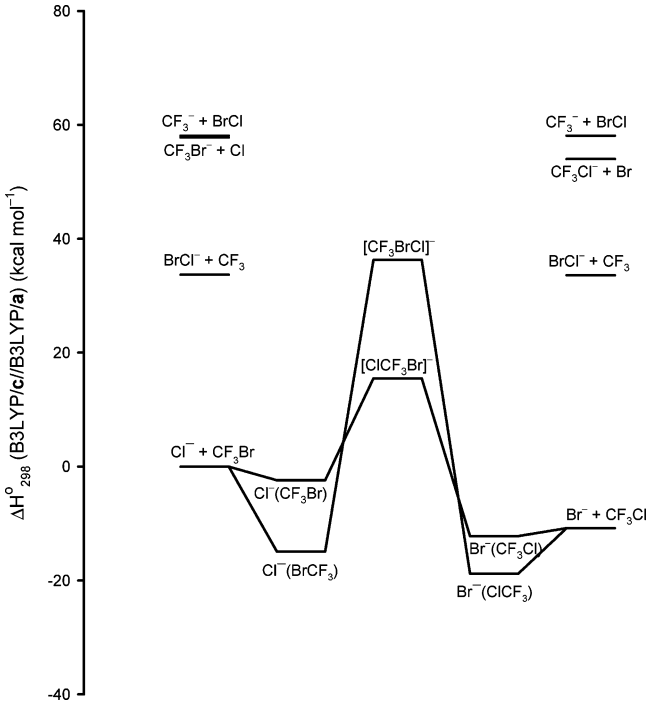

Figure 11. Schematic B3LYP/**c**//B3LYP/**a** potential energy profile for the various $Cl^- + CF_3Br$ and $Br^- + CF_3Cl$ reactions.

$X^-(CF_3Y)$ complexes shows a very different picture. No charge transfer from X^- to CF_3Y takes place. In addition, the charges on the fluorine atoms become somewhat less negative, around $-0.31e$, while the NPA charge on Y becomes negative. The charge on carbon becomes slightly more positive.

More interesting are the charges in the back- and front-side attack transition states. The wave function for the transition state $[XCF_3Y]^{-‡}$ can be viewed, in valence bond terms, as a triple ion configuration, $X^-CF_3^+Y^-$ and the transition state can be represented as a CF_3^+ transfer from X^- to Y^-. In all $[XCF_3Y]^{-‡}$ transition states investigated, the B3LYP/**a** NPA charges on X and Y are $-0.70e$, while on the CF_3 moiety it is $+0.40e$ ($q(C)$ $\sim +1.25e$ and $q(F) \sim -0.27e$). Unlike the situation for the $[XCH_3Y]^{-‡}$ transition states, where a decrease in $|q(CH_3)|^{1/2}$ was observed going from $[ClCH_3Cl]^{-‡}$ to $[BrCH_3Br]^{-‡}$,[37] here no decrease is observed in $|q(CF_3)|^{1/2}$. In the $[CF_3XY]^{-‡}$ transition states a very different picture emerges. Both X and Y have NPA charges around $-0.48e$, thereby making the CF_3 moiety neutral, with $q(C) = +1.05e$ and $q(F) = -0.37e$. This thus also supports the $[CF_3^{\bullet}\ XY^{-\bullet}]^{‡}$ description of the $[CF_3XY]^{-‡}$ transition state.

Finally, in $[BrCF_2Cl_2]^{-‡}$ and $[CF_2Cl_2Br]^{-‡}$, the only change in the various NPA charges arising from substitution of a fluorine atom by a chlorine atom is at the carbon atom. In the first transition state it is $+0.80e$, while in the second it is $+0.66e$. The new chlorine atoms have an NPA charge of $+0.14e$ and $0.00e$, respectively.

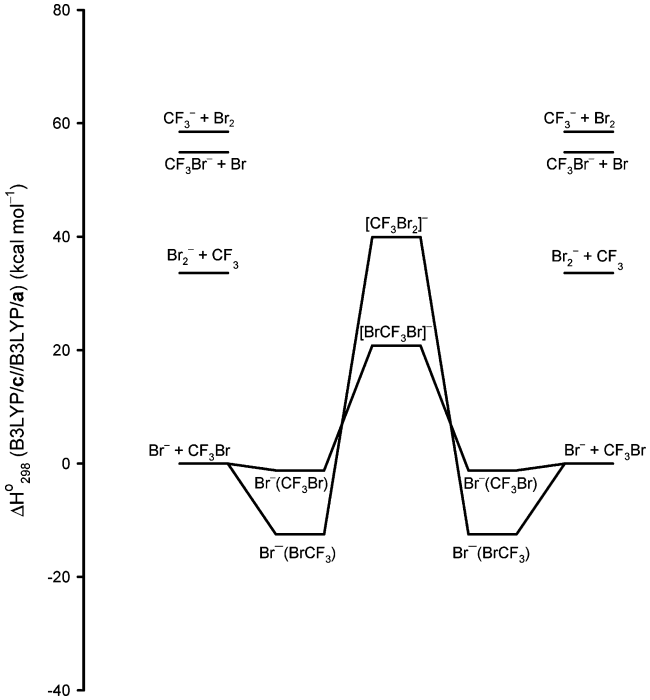

Figure 12. Schematic B3LYP/**c**//B3LYP/**a** potential energy profile for the various$Br^- + CF_3Br$ reactions.

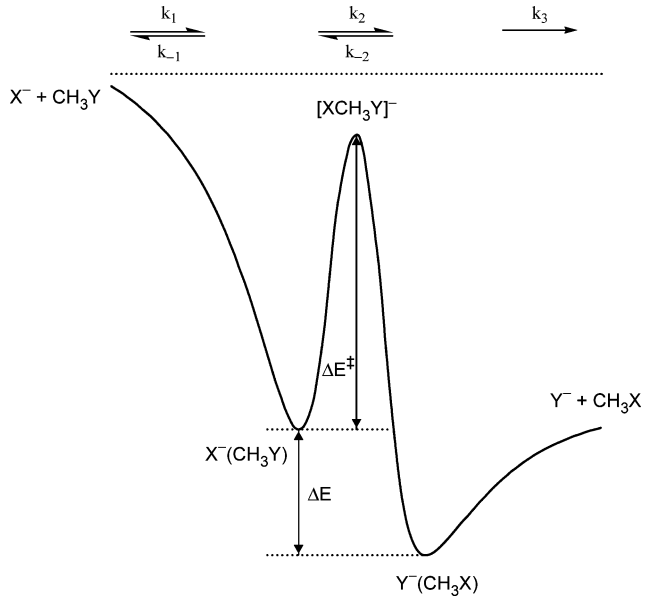

Figure 13. Schematic double well gas-phase S_N2 potential energy profile with the definitions of ΔE and $\Delta E^{\#}$ for the Marcus equation.

TABLE 11: Computational B3LYP/a (b for Y = I) and Experimental Normal Mode Vibrational Frequencies for CF_3Y (Y = Cl, Br, I)

	$\nu(CF_3Cl)^a$		$\nu(CF_3Br)^a$		$\nu(CF_3I)^a$	
normal mode	B3LYP/**a**	experiment[b]	B3LYP/**a**	experiment[b]	B3LYP/[**a**/**b**]	experiment[b]
CX bend	344	350	300	306	266	260
CX bend	344	350	300	306	266	260
CF_3 s-deform	462	476	339	349	276	286
CF_3 d-deform	553	563	541	547	531	537
CF_3 d-deform	553	563	541	547	531	537
CX str	772	781	750	760	735	742
CF_3 s-str	1074	1105	1057	1089	1048	1080
CF_3 d-str	1180	1212	1174	1210	1154	1187
CF_3 d-str	1180	1212	1174	1210	1154	1187

[a] In cm^{-1}. [b] From ref 117.

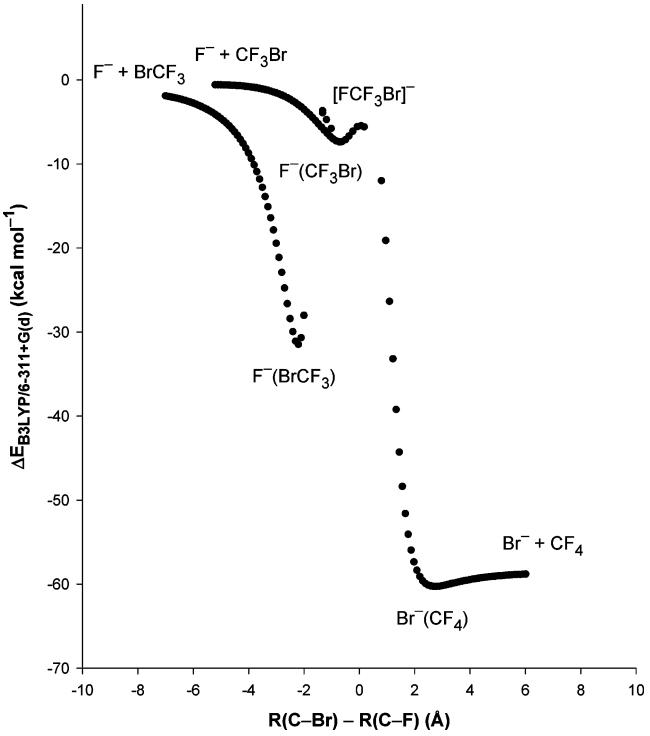

Figure 14. Possible B3LYP/**a** potential energy profiles for the $F^- + CF_3Br \rightarrow Br^- + CF_4$ and $F^- + CF_3Br \rightleftharpoons F^-(BrCF_3)$ reactions.

5. Potential Energy Surfaces. Morris and Viggiano have previously investigated the reactions of F^- with both CF_3Br and CF_3I and found that two reaction channels exist, displacement and association.[91] The observation of these two reactions represented the first clear indications that a CF_3 group need not necessarily prevent back-side attack by a nucleophile in a gas-phase S_N2 reaction. From their extensive studies of temperature, kinetic energy, and pressure dependences of the two reaction channels, they concluded that the two reactions are not competitive and that, unlike the reactions with the analogous CH_3X species, the displacement reaction behaves statistically. The CF_3Br reaction has also been investigated computationally in conjunction with the present work and possible B3LYP/**a** potential energy profiles for the separate reactions of eqs 42 and 43 are shown in Figure 14. The distance $R(C-Br) - R(C-F) = \Delta R$ has been chosen as the reaction coordinate. As

$$F^- + CF_3Br \rightarrow Br^- + CF_4 \qquad (42)$$

$$F^- + CF_3Br \rightarrow F^-(BrCF_3) \qquad (43)$$

expected, the ion−dipole interaction between F^- and $(BrCF_3)$ becomes important even at relatively long ion neutral separations. In contrast to the potential energy profiles shown in Figures 10−12, the substantial exothermicity of eq 42 then also has the effect of lowering the transition state energy below that of the separated reactants. The calculated binding energy of the back-side attack complex of 8.2 kcal mol^{-1} is less than that found, computationally and experimentally, for either $Cl^-(CH_3Cl)$ or $Cl^-(CH_3Br)$, both of which were observed to exhibit nonstatistical S_N2 behavior. Nonstatistical behavior arises when the complex lifetime is too short to permit complete randomization of the internal energy among the vibrational modes of the complex. The unimolecular dissociation lifetimes of nascent ion−molecule complexes such as these are determined by the binding energy, the number of vibrational modes and the vibrational frequencies of the complex. Since the binding energy is less than and the number of normal modes the same as both $Cl^-(CH_3Cl)$ and $Cl^-(CH_3Br)$ it might at first seem unlikely that the back-side attack complex could be solely responsible for the statistical behavior. However in the cases where nonstatistical behavior was observed this was also the result of poor mode coupling between the intermolecular modes of the newly formed complex and the intramolecular modes of the alkyl halide. The front-side attack complex is calculated to be much more strongly bound at 30.9 kcal mol^{-1} and it is almost certainly this species that is observed in the association reaction, eq 43, in the experiments of Morris and Viggiano. They also observe that the rate constant for the association reaction increases with increasing pressure while that for the displacement reaction remains essentially constant. With increasing temperature both rate constants decrease but that for the association reaction decreases more rapidly such that at the higher temperatures the association product represents a smaller fraction of the overall reactivity. These data led Morris and Viggiano to conclude that there were possibly different intermediates involved in the two processes since the increase in formation of the association product did not appear to occur at the expense of the displacement product. Thus, the most plausible explanation of the behavior of this system is that the S_N2 displacement reaction occurs on the back-side attack potential energy surface while the complex formation occurs on the front-side attack surface. As expected, the well-depth for the $Br^-(CF_4)$ exit channel complex is very shallow.

It is also of interest to consider the potential energy profile for back-side attack in the $Cl^- + CF_3Cl$ system using the same type of reaction coordinate, as shown in Figure 15. Ervin and co-workers[25b,c] have recently shown that for endothermic S_N2 reactions the reaction threshold observed can exhibit a considerable excess translational energy requirement above the thermodynamic threshold, even when the central barrier lies below this threshold. The close resemblance of this surface to that of

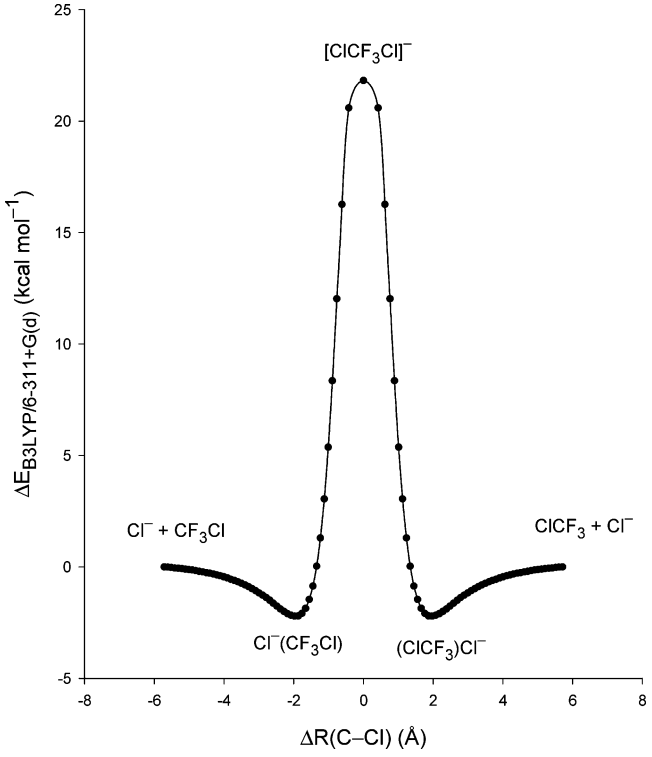

Figure 15. B3LYP/**a** potential energy profile for the $Cl^- + CF_3Cl \rightarrow [ClCF_3Cl]^{-\ddagger} \rightarrow ClCF_3 + Cl^-$ back-side attack S_N2 reaction.

condensed phase systems renders this reaction a potentially interesting gas phase analogue. It would thus be of some interest to perform GIB experiments on systems such as those investigated here involving trifluoromethyl halides. These systems have central barriers well above the thermodynamic threshold and it would be of interest to use such experiments to determine whether the transition states might be energetically located. This is essentially the type of experiment performed previously by Hop and McMahon,[88] albeit with much less precision, for the analogous endothermic reaction given by eq 15. As shown by the data in Table 10, the threshold found in that case is in very good agreement with that calculated in the present work for the energy of the back-side attack transition state. This would indicate that the application of the GIB threshold experiment for S_N2 displacement reactions and halogen abstraction reactions might yield accurate energetics for the back-side and front-side attack transition states, respectively.

Conclusion

The B3LYP/**a** level of theory has been shown to be valuable for calculation of structures, dipole moments, and normal mode vibrational frequencies of CF_3X (X = F, Cl, Br, I) that are in good agreement with experimental data. Two stable isomeric types of cluster ion of the halide ions with the trifluoromethyl halides have been found, $X^-(YCF_3)$ and $X^-(CF_3Y)$. These correspond to front-side and back-side attack S_N2 reaction mechanism complexes, respectively. Associated with these two different mechanisms are two transition state structures, $[CF_3XY]^{-\ddagger}$ and $[XCF_3Y]^{-\ddagger}$, respectively.

From PHPMS experiments, ΔH and ΔS values for the formation of the $Cl^-(BrCF_3)$, $Cl^-(ICF_3)$ (ΔH only), and $Br^-(BrCF_3)$ complexes were determined. There was good agreement with ΔH°_{298} values from B3LYP/**c**//B3LYP/**a** computations, and ΔS°_{298} values from the B3LYP/**a** computations. In addition to the thermochemistry of the S_N2 reactions, the thermochemistry of other, higher energy pathways were also determined. The agreement of the B3LYP/**c**//B3LYP/**a** computations when the reaction includes radicals and radical anions is less good than that in the case of closed shell species. It has been shown that the S_N2 reaction between a halide ion and a trifluoromethyl halide proceeds preferentially through a back-side attack transition state. The $Cl^- + CF_3Br \rightarrow Br^- + CF_3Cl$ has been shown to obey Marcus theory, which means that even at high kinetic energies the back-side S_N2 reaction may be initiated by electron transfer. From normal mode vibrational analysis and NPA charges it has been shown that the $[CF_3XY]^{-\ddagger}$ transition state closely resembles a $[CF_3^\bullet\ XY^{-\bullet}]^\ddagger$ complex.

Finally, potential energy surfaces have been determined for several reactions as well as clustering equilibria. The suggestion by Morris and Viggiano that the formation of Br^- from the reaction between F^- and CF_3Br comes from back-side nucleophilic displacement is shown to likely be correct, demonstrating that the CF_3 group does not necessarily hinder attack on the carbon atom despite the presence of three electronegative fluorine atoms. At threshold, the back-side S_N2 reaction between kinetically excited Cl^- and CF_3Cl should also proceed through a $[ClCF_3Cl]^{-\ddagger}$ transition state.

Acknowledgment. The authors thank the Natural Sciences and Engineering Research Council of Canada (NSERC) and the donors of the Petroleum Research Fund, administered by the American Chemical Society, for financial support.

References and Notes

(1) Bohme, D K.; Young, L. B. *J. Am. Chem. Soc.* **1970**, *92*, 7354.
(2) Young, L. B.; Lee-Ruff, E.; Bohme, D. K. *Chem. Commun.* **1973**, 35.
(3) Bohme, D. K.; Mackay, G. I.; Payzant, J. D. *J. Am. Chem. Soc.* **1974**, *96*, 4027.
(4) Tanaka, K.; Mackay, G. I.; Payzant, J. D.; Bohme, D. K. *Can. J. Chem.* **1976**, *54*, 1643.
(5) Brauman, J. I.; Olmstead, W. M.; Lieder, C. A. *J. Am. Chem. Soc.* **1974**, *96*, 4030.
(6) Olmstead, W. N.; Brauman, J. I. *J. Am. Chem. Soc.* **1977**, *99*, 4219 and references therein.
(7) Caldwell, G.; Magnera, T. F.; Kebarle, P. *J. Am. Chem. Soc.* **1984**, *106*, 959.
(8) De Puy, C. H.; Gronert, S.; Mullin, A.; Bierbaum, V. M. *J. Am. Chem. Soc.* **1990**, *112*, 8650.
(9) Wladkowski, B. D.; Brauman, J. I. *J. Phys. Chem.* **1993**, *97*, 13158 and a reference therein.
(10) Knighton, W. B.; Bognar, J. A.; O'Connor, P. M.; Grimsrud, E. P. *J. Am. Chem. Soc.* **1993**, *115*, 12079 and references therein.
(11) Cyr, D. M.; Scarton, M. G.; Johnson, M. A. *J. Chem. Phys.* **1993**, *99*, 4869.
(12) Viggiano, A. A.; Morris, R. A.; Su, T. *J. Am. Chem. Soc.* **1994**, *116*, 2213.
(13) Graul, S. T.; Bowers, M. T. *J. Am. Chem. Soc.* **1994**, *116*, 3875 and references therein.
(14) Li, C.; Ross, P.; Szulejko, J. E.; McMahon, T. B. *J. Am. Chem. Soc.* **1996**, *118*, 9360 and references therein.
(15) DeTuri, V. F.; Hintz, P. A.; Ervin, K. E. *J. Phys. Chem. A* **1997**, *101*, 5969 and references therein.
(16) Craig, S. L.; Brauman, J. I. *Science* **1997**, *276*, 1536 and references therein.
(17) Dessent, C. E. H.; Johnson, M. A. *J. Am. Chem. Soc.* **1997**, *119*, 5067.
(18) Lehman, L.; Matejcik, S.; Illenberger, E. *Ber. Bunsen-Ges. Phys. Chem.* **1997**, *101*, 287.
(19) Ayotte, P.; Kim, J.; Kelley, J. A.; Nielsen, S. B.; Johnson, M. A. *J. Am. Chem. Soc.* **1999**, *121*, 6950 and references therein.
(20) Kuznetsov, A. M. *J. Phys. Chem. A* **1999**, *103*, 1239.
(21) Flores, A. E.; Gronert, S. *J. Am. Chem. Soc.* **1999**, *121*, 2627.
(22) Lehman, L.; Illenberger, E. *Int. J. Mass Spectrom.* **1999**, *185/186/187*, 463.
(23) Bierbaum, V. M.; Davico, G. E. *J. Am. Chem. Soc.* **2000**, *122*, 1740.
(24) Langer, J.; Matejcik, S.; Illenberger, E. *Phys. Chem. Chem. Phys.* **2000**, *2*, 1001.

(25) (a) Angel, L. A.; Ervin, K. M. *J. Phys. Chem. A* **2001**, *105*, 4042. (b) Angel, L. A.; Garcia, S. P.; Ervin, K. M. *J. Am. Chem. Soc.* **2002**, *124*, 336. (c) Angel, L. A.; Ervin, K. M. *J. Phys. Chem. A* **2004**, *108*, 9827.

(26) Shi, Z.; Boyd, R. J. *J. Am. Chem. Soc.* **1989**, *111*, 1575 and references therein.

(27) Tucker, S. C.; Truhlar, D. G. *J. Phys. Chem.* **1989**, *93*, 8138 and references therein.

(28) Zulicke, L.; Vetter, R. *J. Am. Chem. Soc.* **1990**, *112*, 5136.

(29) Shi, Z.; Boyd, R. J. *J. Am. Chem. Soc.* **1990**, *112*, 6789.

(30) Shi, Z.; Boyd, R. J. *J. Am. Chem. Soc.* **1991**, *113*, 1072.

(31) Shi, Z.; Boyd, R. J. *J. Am. Chem. Soc.* **1991**, *113*, 2434.

(32) Gronert, S. *J. Am. Chem. Soc.* **1991**, *113*, 6041.

(33) Jensen, F. *Chem. Phys. Lett.* **1992**, *196*, 368.

(34) Lee, I.; Kim, C. K.; Lee, B.-S. *J. Org. Chem.* **1994**, *59*, 4490.

(35) Wladkowski, B. D.; Allen, W. D.; Brauman, J. I. *J. Phys. Chem.* **1994**, *98*, 13532.

(36) Deng, L.; Branchadell, V.; Ziegler, T. *J. Am. Chem. Soc.* **1994**, *116*, 10645.

(37) Glukhotsev, M. N.; Pross, A.; Radom, L. *J. Am. Chem. Soc.* **1995**, *117*, 2024.

(38) Li, G.; Hase, W. L. *J. Am. Chem. Soc.* **1999**, *121*, 7124.

(39) Glukhotsev, M. N.; Pross, A.; Schlegel, H. B.; Bach, R. B.; Radom, L. *J. Am. Chem. Soc.* **1996**, *118*, 11258 and references therein.

(40) Glukhotsev, M. N.; Bach, R. D.; Pross, A.; Radom, L. *Chem. Phys. Lett.* **1996**, *260*, 558.

(41) McKee, M. L. *J. Org. Chem.* **1997**, *62*, 7942.

(42) Uggerud, E. *J. Chem. Soc., Perkin Trans.* **1999**, 1459.

(43) Hoz, S.; Basch, H.; Wolk, J. L.; Hoz, T.; Rozental, E. *J. Am. Chem. Soc.* **1999**, *121*, 7724.

(44) Gronert, S.; Fong, L.-M. *Int. J. Mass Spectrom.* **1999**, *192*, 185.

(45) Moliner, V.; Williams, I. H. *J. Am. Chem. Soc.* **2000**, *122*, 10895.

(46) Safi, B.; Choho, K.; Geerlings, P. *J. Phys. Chem. A* **2001**, *105*, 591.

(47) Parthiban, S.; de Oliveira, G.; Martin, J. M. L. *J. Phys. Chem. A* **2001**, *105*, 895 and references therein.

(48) Vande Linde, S. R.; Hase, W. L. *J. Phys. Chem.* **1990**, *94*, 2778 and references therein.

(49) Vande Linde, S. R.; Hase, W. L. *J. Phys. Chem.* **1990**, *94*, 6148.

(50) Tucker, S. C.; Truhlar, D. G. *J. Am. Chem. Soc.* **1990**, *112*, 3338.

(51) Hase, W. L.; Cho, Y. J. *J. Chem. Phys.* **1993**, *98*, 8626.

(52) Wang, H.; Peslherbe, G. H.; Hase, W. L. *J. Am. Chem. Soc.* **1994**, *116*, 9644.

(53) Wang, H.; Zhu, L.; Hase, W. L. *J. Phys. Chem.* **1994**, *98*, 1608.

(54) Hase, W. L. *Science* **1994**, *266*, 998.

(55) Peslherbe, G. H.; Wang, H.; Hase, W. L. *J. Chem. Phys.* **1995**, *102*, 5626.

(56) Wang, H.; Hase, W. L. *J. Am. Chem. Soc.* **1995**, *117*, 9347 and references therein.

(57) Hu, W.-P.; Truhlar, D. G. *J. Am. Chem. Soc.* **1995**, *117*, 10726.

(58) Wang, H.; Hase, W. L. *Chem. Phys.* **1996**, *212*, 247.

(59) Peslherbe, G. H.; Wang, H.; Hase, W. L. *J. Am. Chem. Soc.* **1996**, *118*, 2257.

(60) Wang, H.; Goldfield, E. M.; Hase, W. L. *J. Chem. Soc., Faraday Trans.* **1997**, 737 and references therein.

(61) Wang, H.; Hase, W. L. *J. Am. Chem. Soc.* **1997**, *119*, 3093 and references therein.

(62) Mann, D. J.; Hase, W. L. *J. Phys. Chem. A* **1998**, *102*, 6208.

(63) Su, T.; Wang, H.; Hase, W. L. *J. Phys. Chem. A* **1998**, *102*, 9819 and references therein.

(64) Igarashi, M.; Tachikawa, H. *Int. J. Mass Spectrom. Ion. Processes* **1998**, *181*, 151.

(65) Li, G.; Hase, W. L. *J. Am. Chem. Soc.* **1999**, *121*, 7124 and references therein.

(66) Raugei, S.; Cardini, G.; Schettino, V. *J. Chem. Phys.* **1999**, *111*, 10887 and references therein.

(67) Hernández, M. I.; Campos-Martínez, J.; Villarreal, P.; Schmatz, S.; Clary, D. C. *Phys. Chem. Chem. Phys.* **1999**, *1*, 1197.

(68) Ervin, K. M. *Int. J. Mass Spectrom.* **1999**, *185/186/187*, 343.

(69) Schmatz, S. *Chem. Phys. Lett.* **2000**, *330*, 188.

(70) Gleave, J. L.; Hughes, E. D.; Ingold, C. K. *J. Chem. Soc.* **1935**, 236.

(71) Ingold, C. K. *Structure and Reactivity in Organic Chemistry*, 2nd ed.; Cornell University Press: Ithaca, NY, 1969.

(72) Hartshorn, S. R. *Aliphatic Nucleophilic Substitution*; Cambridge University Press: London, 1973.

(73) Streitweiser, A., Jr. *Solvolytic Displacement Reactions*; McGraw-Hill: New York, 1973.

(74) Viggiano, A. A.; Morris, R. A.; Paschkewitz, J. S.; Paulson, J. *J. Am. Chem. Soc.* **1992**, *114*, 10477.

(75) Seeley, J.; Morris, R. A.; Viggiano, A. A.; Wang, H.; Hase, W. L. *J. Am. Chem. Soc.* **1997**, *119*, 571.

(76) Craig, S. L.; Zhong, M.; Brauman, J. I. *J. Am. Chem. Soc.* **1998**, *120*, 12125.

(77) Angel, L. A.; Ervin, K. M. *J. Am. Chem. Soc.* **2003**, *125*, 1014.

(78) Tonner, D. S.; McMahon, T. B. *J. Am. Chem. Soc.* **2000**, *122*, 8783.

(79) Barlow, S. E.; Van Doren, J. M.; Bierbaum, V. M. *J. Am. Chem. Soc.* **1988**, *110*, 7240.

(80) Cyr, D. M.; Scarton, M. G.; Wiberg, K. B.; Johnson, M. A.; Nonose, S.; Hirokawa, J.; Tanaka, H.; Kondow, T.; Morris, R. A.; Viggiano, A. A. *J. Am. Chem. Soc.* **1995**, *117*, 7, 1828.

(81) Cyr, D. M.; Posey, L. A.; Bishea, G. A.; Han, C.-C.; Johnson, M. A. *J. Am. Chem. Soc.* **1991**, *113*, 9697.

(82) Cyr, D. M.; Bishea, G. A.; Scarton, M. G.; Johnson, M. A. *J. Chem. Phys.* **1992**, *97*, 5991.

(83) Cyr, D. M.; Bishea, G. A.; Han, C.-C.; Posey, L. A.; Johnson, M. A. *Soc. Photo-Opt. Instrum. Eng. (SPIE) Proc.* **1992**, *1638*, 74.

(84) Artau, A.; Nizzi, K. A.; Hill, B. T.; Sunderlin, L. S.; Wenthold, P. G. *J. Am. Chem. Soc.* **2000**, *122*, 10667.

(85) Nizzi, K. E.; Pommerening, C. A.; Sunderlin, L. S. *J. Phys. Chem. A* **1998**, *102*, 7674.

(86) Nizzi, K. E.; Pommerening, C. A.; Sunderlin, L. S. Do, K.; Klein, T. P.; Pommerening, C. A.; Sunderlin, L. S. *J. Am. Soc. Mass Spectrom.* **1997**, *8*, 688.

(87) Sanov, A.; Sanford, T.; Butler, L. J.; Vala, J.; Kosloff, R.; Lineberger, W. C. *J. Phys. Chem. A* **1999**, *103*, 10244.

(88) Hop, C. E. C. A.; McMahon, T. B. *J. Phys. Chem.* **1991**, *95*, 10582.

(89) Sunderlin, L. S.; Aristov, N.; Armentrout, P. B. *J. Am. Chem. Soc.* **1987**, *109*, 78 and references therein.

(90) Morris, R. A. *J. Chem. Phys.* **1992**, *97*, 2372.

(91) Morris, R. A.; Viggiano, A. A. *J. Phys. Chem.* **1994**, *98*, 3740.

(92) Morris, R. A.; Viggiano, A. A.; Miller, T. M.; Seeley, J. V.; Arnold, S. T.; Paulson, J. F.; Van Doren, J. M. *J. Phys. Chem.* **1996**, *100*, 10641.

(93) Staneke, P. O.; Groothuis, G.; Ingemann, S.; Nibbering, N. M. M. *Int. J. Mass Spectrom. Ion Processes* **1995**, *149/150*, 99.

(94) Szulejko, J. E.; Fisher, J. J.; McMahon, T. B.; Wronka, J. *Int. J. Mass Spectrom. Ion Processes* **1988**, *83*, 147.

(95) Frisch, M. J.; Trucks, G. W.; Schlegel, H. B.; Gill, P. M. W.; Johnson, B. G.; Robb, M. A.; Cheeseman, J. R.; Keith, T.; Petersson, G. A.; Montgomery, J. A.; Raghavachari, K.; Al-Laham, M. A.; Zakrzewski, V. G.; Ortiz, J. V.; Foresman, J. B.; Peng, C. Y.; Ayala, P. Y.; Chen, W.; Wong, M. W.; Andres, J. L.; Replogle, E. S.; Gomperts, R.; Martin, R. L.; Fox, D. J.; Binkley, J. S.; Defrees, D. J.; Baker, J.; Stewart, J. P.; Head-Gordon, M.; Gonzales, C.; Pople, J. A. *Gaussian 94*, Revision B3; Gaussian Inc.: Pittsburgh, PA, 1995.

(96) Frisch, M. J.; Trucks, G. W.; Schlegel, H. B.; Scuseria, G. E.; Robb, M. A.; Cheeseman, J. R.; Zakrzewski, V. G.; Montgomery, J. A., Jr.; Stratmann, R. E.; Burant, J. C.; Dapprich, S.; Millam, J. M.; Daniels, A. D.; Kudin, K. N.; Strain, M. C.; Farkas, O.; Tomasi, J.; Barone, V.; Cossi, M.; Cammi, R.; Mennucci, B.; Pomelli, C.; Adamo, C.; Clifford, S.; Ochterski, J.; Petersson, G. A.; Ayala, P. Y.; Cui, Q.; Morokuma, K.; Malick, D. K.; Rabuck, A. D.; Raghavachari, K.; Foresman, J. B.; Cioslowski, J.; P.; Ortiz, J. V.; Baboul, A. G.; Stefanov, B. B.; Liu, G.; Liashenko, A.; Piskorz, P.; Komaromi, I.; Gomperts, R.; Martin, R. L.; Fox, D. J.; Keith, T.; Al-Laham, M. A.; Peng, C. Y.; Nanayakkara, A.; Gonzalez, C.; Challacombe, M.; Gill, M. W.; Johnson, B.; Chen, W.; Wong, M. W.; Andres, J. L.; Gonzalez, C.; Head-Gordon, M.; Replogle, E. S.; Pople, J. A. *Gaussian 98*, Revision A.7 Gaussian, Inc., Pittsburgh, PA, 1998.

(97) Lee, C.; Yang, W.; Parr, R. G. *Phys. Rev. B* **1988**, *37*, 785.

(98) Becke, A. D. *J. Chem. Phys.* **1993**, *98*, 1372, 5648.

(99) Krishnan, R.; Binkley, J. S.; Seeger, R.; Pople, J. A. *J. Chem. Phys.* **1980**, *72*, 650.

(100) Clark, T.; J. Chandrasekhar, J.; Schleyer, P.v. R. *J. Comput. Chem.* **1983**, *4*, 294.

(101) Hay P. J.; Wadt, W. R. *J. Chem. Phys.* **1985**, *82*, 284.

(102) Reed, A. E.; Curtiss, L. A.; Weinhold, F. *Chem. Rev.* **1988**, *88*, 899 and references therein.

(103) Krishnan, R.; Binkley, J. S.; Seeger, R.; Pople, J. A. *J. Chem. Phys.* **1980**, *72*, 650.

(104) Clark, T.; Chandrasekhar, J.; Spitznagel, G. W.; Schleyer, P. v. R. *J. Comput. Chem.* **1983**, *4*, 294.

(105) Gill, P. M. W.; Johnson, B. G.; Pople, J. A.; Frisch, M. J. *Chem. Phys. Lett.* **1992**, *197*, 499.

(106) Frisch, M. J.; Pople, J. A.; Binkley, J. S. *J. Chem. Phys.* **1984**, *80*, 3265.

(107) Møller, C.; Plesset, M. S. *Phys. Rev.* **1934**, *46*, 618.

(108) Glukhovtsev, M. N.; Pross, A.; McGrath, M. P. Radom, L. *J. Chem. Phys.* **1995**, *103*, 1878.

(109) Curtiss, L. A.; Raghavachari, K.; Redfern, P. C.; Rassolov, V.; Pople, J. A. *J. Chem. Phys.* **1998**, *109*, 7764.

(110) Bartell, L. S.; Brockway, L. O. *J. Chem. Phys.* **1955**, *23*, 1860.

(111) Bowen, H. J. M. *Trans. Faraday Soc.* **1954**, *50*, 444.

(112) Wong, C.; Schomaker, V. *J. Chem. Phys.* **1958**, *28*, 1010.

(113) Roszak, S.; Koski, W. S.; Kaufman, J. J.; Balasubramanian, K. *J. Chem. Phys.* **1997**, *106*, 7709.

(114) *CRC Handbook of Chemistry and Physics*, 76th ed.; Lide, D. L., Ed.; CRC: Boca Raton, FL, 1995.

(115) Herzberg, G. *Molecular Spectra and Molecular Structure, I. Spectra of Diatomic Molecules*, 2nd ed.; Van Nostrand Reinhold Co.: New York, 1950.
(116) Marcus, R. A. *Annu. Rev. Phys. Chem.* **1964**, *15*, 155.
(117) Pellerite, M. J.; Brauman, J. I. *J. Am. Chem. Soc.* **1980**, *102*, 5993.
(118) Pellerite, M. J.; Brauman, J. I. *J. Am. Chem. Soc.* **1983**, *105*, 2672.
(119) Dodd, J. A.; Brauman, J. I. *J. Am. Chem. Soc.* **1984**, *106*, 5356.
(120) Dodd, J. A.; Brauman, J. I. *J. Phys. Chem.* **1986**, *90*, 3559.
(121) Wolfe, S.; Mitchell, D. J.; Schlegel, H. B. *J. Am. Chem. Soc.* **1981**, *103*, 7692.
(122) Wolfe, S.; Mitchell, D. J.; Schlegel, H. B. *J. Am. Chem. Soc.* **1981**, *103*, 7694.
(123) Shaik, S. S.; Pross, A. *J. Am. Chem. Soc.* **1982**, *104*, 2708.
(124) Albery, W. J.; Kreevoy, M. M. *Adv. Phys. Org. Chem.* **1978**, *16*, 87.
(125) http://webbook.nist.gov/chemistry/.
(126) Shimanouchi, T. *Tables of Molecular Vibrational Frequencies Consolidated Volume I*; National Bureau of Standards: Washington, DC, 1972; p 1.
(127) Batana, A.; Bruno, J.; Munn, R. W. *Mol. Phys.* **1997**, *92*, 1029.
(128) The cross section of CF_3Cl was estimated from the experimental cross sections of CCl_4,[120] CCl_3F,[121] CCl_2F_2,[122] and CF_4.[123]
(129) Landolt-Börnstein. *Physikalisch-Chemische Tabellen*; Springer: Berlin.
(130) *Thermodynamic Properties of Trichloromonofluoromethane*; Kinetic Chemical, Inc.: 1938.
(131) *Thermodynamic Properties of Dichlorodifluoromethane*, Circular 12; American Society of Refrigerating Engineers: New York, 1931.
(132) MacCormack, K. E.; Schneider, W. G. *J. Chem. Phys.* **1951**, *19*, 849.
(133) Deyerl, H.-J.; Alconcel, L. S.; Continetti, R. E. *J. Phys. Chem. A* **2001**, *105*, 552.